

An Expressive Ansatz for Low-Depth Quantum Approximate Optimisation

V Vijendran^{1,2,*}, Aritra Das^{1,†}, Dax Enshan Koh^{3,‡}, Syed M Assad^{1,2,§} and Ping Koy Lam^{1,2,¶}

¹*Centre for Quantum Computation and Communication Technologies (CQC2T),
Department of Quantum Science, Research School of Physics and Engineering,
Australian National University, Acton 2601, Australia*

²*A*STAR Quantum Innovation Centre (Q.InC), Institute of Materials Research and Engineering (IMRE),
Agency for Science, Technology and Research (A*STAR), 2 Fusionopolis Way,
Innovis #08-03, Singapore 138634, Republic of Singapore*

³*A*STAR Quantum Innovation Centre (Q.InC), Institute of High Performance Computing (IHPC),
Agency for Science, Technology and Research (A*STAR), 1 Fusionopolis Way,
#16-16 Conneris, Singapore 138632, Republic of Singapore*

The Quantum Approximate Optimisation Algorithm (QAOA) is a hybrid quantum-classical algorithm used to approximately solve combinatorial optimisation problems. It involves multiple iterations of a parameterised ansatz that consists of a problem and mixer Hamiltonian, with the parameters being classically optimised. While QAOA can be implemented on near-term quantum hardware, physical limitations such as gate noise, restricted qubit connectivity, and state-preparation-and-measurement (SPAM) errors can limit circuit depth and decrease performance. To address these limitations, this work introduces the eXpressive QAOA (XQAOA), an overparameterised variant of QAOA that assigns more classical parameters to the ansatz to improve its performance at low depths. XQAOA also introduces an additional Pauli-Y component in the mixer Hamiltonian, allowing the mixer to implement arbitrary unitary transformations on each qubit. To benchmark the performance of XQAOA at unit depth, we derive its closed-form expression for the MaxCut problem and compare it to QAOA, Multi-Angle QAOA (MA-QAOA) [Sci Rep 12, 6781 (2022)], a Classical-Relaxed algorithm, and the state-of-the-art Goemans-Williamson algorithm on a set of unweighted regular graphs with 128 and 256 nodes for degrees ranging from 3 to 10. Our results indicate that at unit depth, XQAOA has benign loss landscapes with local minima concentrated near the global optimum, allowing it to consistently outperform QAOA, MA-QAOA, and the Classical-Relaxed algorithm on all graph instances and the Goemans-Williamson algorithm on graph instances with degrees greater than 4. Small-scale simulations also reveal that unit-depth XQAOA invariably surpasses both QAOA and MA-QAOA on all tested depths up to five. Additionally, we find an infinite family of graphs for which XQAOA solves MaxCut exactly and analytically show that for some graphs in this family, special cases of XQAOA are capable of achieving a much larger approximation ratio than QAOA. Overall, XQAOA is a more viable choice for variational quantum optimisation on near-term quantum devices, offering competitive performance at low depths.

I. INTRODUCTION

Full-fledged fault-tolerant quantum computers capable of executing quantum algorithms that can solve problems of interest are expected to involve at least millions of physical qubits, high-fidelity gate operations, and quantum error correction techniques [1]. While the physical realisation of such devices is still a long way off, noisy intermediate-scale quantum (NISQ) devices capable of running quantum algorithms with limited circuit depth are becoming more widely available [2, 3]. Particularly promising are the variational quantum algorithms (VQAs) [4–8] capable of potentially realising a quantum advantage on NISQ devices. Unlike traditional quantum algorithms like Shor’s algorithm [9] that use specially designed quantum circuits to solve specific problems, VQAs

use parameterised quantum circuits whose objective is to drive a quantum state close to the desired state that minimises a cost function by varying the gate parameters.

The Quantum Approximate Optimisation Algorithm (QAOA) [8] is one such algorithm that can solve optimisation problems by encoding their solutions into the ground state of a quantum Hamiltonian and preparing a quantum state that approximates this ground state. QAOA involves a p -level quantum circuit described by a collection of $2p$ classical parameters to generate a quantum state. The classical parameters are fine-tuned to optimise the expectation of the cost for the generated quantum state. This quantum state can then be measured to obtain an approximate solution to the optimisation problem. Besides its ability to solve combinatorial optimisation problems, QAOA can be used to perform universal quantum computation [10, 11]. Moreover, even at its lowest level $p = 1$, QAOA can efficiently generate probability distributions that likely cannot be generated efficiently by classical computers [12, 13].

Several variants of the original QAOA algorithm have been developed, each with different operators and initial states [14–26] or different objective functions for tun-

* v.vijendran@anu.edu.au

† aritra.das@anu.edu.au

‡ dax_koh@ihpc.a-star.edu.sg

§ cqtsma@gmail.com

¶ pingkoy@imre.a-star.edu.sg

ing the variational parameters [27, 28]. Depth-reduction techniques [29, 30] or methods like circuit cutting [31, 32] that optimise QAOA circuits while taking into account quantum hardware limitations; as well as classical aspects such as hyper-parameter optimisation and exploitation of problem structure, have been studied as well [18, 19, 33–40]. However, one key drawback of realistic QAOA implementations is the need for deep quantum circuits with many qubits [41–46]. This poses a hurdle since NISQ devices are significantly limited due to their restricted qubit connectivity, inadequate qubit control, limited coherence times, and absence of quantum error correction, causing noise to grow with circuit depth and eventually affecting the fidelity of the resulting quantum state [47–56].

There are several approaches that have been proposed to improve the performance of low-depth QAOA by adding new parameters to the ansatz [23, 57–61]. These approaches include Multi-Angle QAOA (MA-QAOA) [57], which increases the number of classical parameters added in each layer for more precise control of the optimisation process; Free-Axis Mixer QAOA (FAM-QAOA) [58], which includes additional variational parameters in the mixer Hamiltonian that allow for rotation about an axis in the XY plane; QAOA with Adaptive Bias Fields (AB-QAOA) [59], which adds a Pauli-Z component to the mixer Hamiltonian; Adaptive Derivative Assembled Problem Tailored QAOA (ADAPT-QAOA) [60], which grows the ansatz iteratively using a gradient criterion; and QAOA+ [23], which augments the traditional QAOA ansatz with an additional multi-parameter layer that is independent of the specific problem being solved. Despite these improvements, there remains an imperative for problem-inspired quantum ansatzes with minimal computational overhead, which are not only expressive but also readily trainable allowing for greater flexibility in the optimisation process.

This paper presents a modified version of the QAOA called eXpressive QAOA (XQAOA). It shares the same inspiration behind the recently proposed Multi-Angle QAOA (MA-QAOA) approach [57] but goes beyond it by including an additional Pauli-Y component in the mixing Hamiltonian. This modification strategically over-parameterises the quantum ansatz, facilitating the exploration of all relevant directions of the Hilbert space by allowing the mixer to effectively implement arbitrary unitary operations on each qubit with just a single iteration. As a result, XQAOA does not suffer from *reachability deficits* [44, 62]; with appropriately chosen angles, XQAOA can output any computational-basis state. To quantify the performance of the quantum algorithm, we apply it to the problem of maximum cut (MaxCut) on arbitrary graphs. We derive closed-form expressions for XQAOA, MA-QAOA, and QAOA at $p = 1$ for the MaxCut problem and benchmark their performance against a naive Classical-Relaxed (CR) algorithm and the state-of-the-art Goemans-Williamson (GW) [63] algorithm on unweighted D -regular graphs—graphs where every node

is connected to D other nodes—with 128 and 256 nodes for $3 \leq D \leq 10$. The benchmark reveals that at $p = 1$, XQAOA outperforms MA-QAOA, QAOA, and the CR algorithm on all graph instances and the GW algorithm on graphs with $D > 4$; interestingly, the CR algorithm also outperforms QAOA and MA-QAOA on all graphs with QAOA matching MA-QAOA’s performance for graphs with $D > 5$. We find that the exceptional performance of the XQAOA ansatz is attributed to the favourable characteristics of its benign loss landscape, which is notably free of barren plateaus and spurious local minima, with any remaining local minima being concentrated around the global optimum. Lastly, we show that for unweighted triangle-free graphs with edges of odd degrees, XQAOA can solve MaxCut exactly. Here, the edge degree $d(e)$ of an edge $e = \{u, v\}$ is defined as the number of neighbours of e , i.e., $d(e) = |\mathcal{N}(u) \cup \mathcal{N}(v)| - 2$, where $\mathcal{N}(w)$ is the set of all nodes connected to the node w .

The structure of the remainder of this paper is as follows: in section II, we review the necessary background material, where we explain the MaxCut problem and the challenges in finding its optimal solution (section II A), the traditional QAOA ansatz and its application to the MaxCut problem (section II B), and the MA-QAOA ansatz and its extension to MaxCut on arbitrary graphs in (section II C). In section III, we introduce XQAOA and discuss its variants and other notable properties. In section IV, we present the results of our numerical simulations. In section V, we interpret and discuss our results, and in section VI, we provide some concluding remarks.

II. PRELIMINARIES

A. Maximum Cut (MaxCut)

Many real-world problems can be phrased as combinatorial optimisation problems [64]. Here, we lay emphasis on XQAOA’s application to an archetypal problem known as MaxCut, which has numerous applications in computer science and operations research, including statistical physics and circuit layout design [65], analysis of social networks [66], data clustering [67], semi-supervised learning [68], and more [69, 70]. The (weighted) MaxCut problem is an optimisation problem in which we are given an undirected weighted graph and asked to partition its vertices into two disjoint sets S and \bar{S} such that the sum of the weights of the edges between the two sets is as large as possible.

Formally, given an undirected graph $G = (V, E)$ and non-negative weights $w_{uv} = w_{vu}$ on the edges $\{u, v\} \in E$, the MaxCut problem is that of finding a set S of vertices that maximises the weight of the edges in the cut (S, \bar{S}) ; that is, the weight of the edges with one endpoint in S and the other in \bar{S} . The MaxCut problem can be

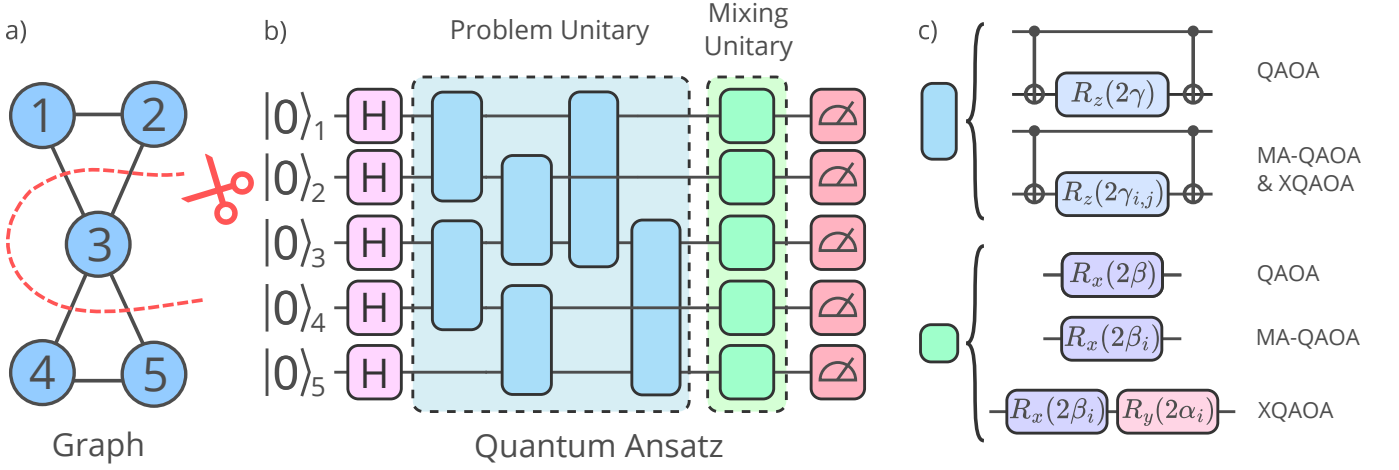


FIG. 1: a) A specific instance of a graph for which we want to identify a set of vertices that maximises the number of edges that are cut. b) A quantum circuit with a single iteration of a quantum ansatz applied to it. The quantum ansatz consists of a unitary operation specific to the problem being solved and a problem-independent mixing unitary. c) Decomposing the problem and mixing unitaries for QAOA, MA-QAOA, and XQAOA into CNOT and single-qubit rotation gates.

formulated as a binary quadratic program of the form

$$\begin{aligned} & \text{Maximise} \quad \sum_{\{u,v\} \in E} \frac{1}{2} w_{uv} (1 - y_u y_v) \\ & \text{s.t} \quad y_u \in \{-1, 1\} \quad \forall u \in V. \end{aligned} \quad (1)$$

The optimisation problem given by eq. (1) is NP-hard¹, which suggests that it is highly plausible that no efficient algorithm exists that can solve it.

However, there are approximation algorithms that can find good solutions in polynomial time for many instances of the problem. The GW algorithm holds the current record for an approximation ratio guarantee on generic graphs, achieving an approximation ratio of $r^* \approx 0.87856$ using semidefinite programming [63]. When confined to unweighted 3-regular graphs, this lower bound can be increased to $r^* \approx 0.9326$ [72]². Assuming the unique games conjecture [74]³ and that $P \neq NP$, this is the best possible approximation ratio for MaxCut [75–77] that polynomial-time classical algorithms can achieve. Additionally, it has

been proven that it is NP-hard to approximate the Max-Cut value with an approximation ratio that is better than $r^* \geq 16/17 \approx 0.94117$ [78, 79].

B. Quantum Approximate Optimisation Algorithm (QAOA)

Combinatorial optimisation problems can be formulated using n bits and m clauses, where each clause represents a constraint on a subset of the bits that is satisfied for certain combinations of values for those bits but not for others. We consider the case when each clause μ is associated with a cost $c_\mu \in \mathbb{R}$. The objective function defined on n -bit strings is then given by the sum of the costs of the satisfied clauses:

$$C(z) = \sum_{\mu=1}^m C_\mu(z), \quad (2)$$

where $z = z_1 z_2 \dots z_n \in \{0, 1\}^n$ is an n -bit string and $C_\mu(z) = c_\mu$ if z satisfies the clause μ and 0 otherwise. An approximate optimisation algorithm aims to find a string z that achieves a desired approximation ratio r^* , i.e., it seeks a string z that satisfies

$$\frac{C(z)}{C_{\max}} \geq r^*, \quad (3)$$

where $C_{\max} = \max_z C(z)$. The QAOA algorithm consists of two operators (see fig. 1): the problem unitary and the mixing unitary, which are generated by the problem Hamiltonian and mixing Hamiltonian, respectively. The problem unitary is defined as the following unitary operator $U(C, \gamma)$ which depends on a real-valued angle

¹ Historically, the NP-hardness of MaxCut was one of the earliest results known in computational complexity theory: the decision version of the MaxCut problem was one of Karp's first NP-complete problems [71]. Here, a decision problem is a problem in which a yes-or-no answer is sought. A decision version of the MaxCut problem may be phrased as follows: given a graph G and an integer j , determine if G has a cut whose size is at least j .

² This bound by Halperin *et al.* is an improvement over an earlier result by Feige *et al.*, who found a smaller lower bound of $r^* \approx 0.924$ for unweighted 3-regular graphs [73].

³ The unique games conjecture asserts that the problem of estimating the approximate value of a certain type of game, known as a unique game, has an NP-Hard computational complexity.

$\gamma \in \mathbb{R}$:

$$U(C, \gamma) = e^{-i\gamma C} = \prod_{\mu=1}^m e^{-i\gamma C_\mu}. \quad (4)$$

The operators $C = \sum_z C(z) |z\rangle\langle z|$ and $C_\mu = \sum_z C_\mu(z) |z\rangle\langle z|$ are the diagonal operators whose entries are the objective function values. Next, the mixing unitary is defined as the β -dependent product of commuting one-qubit unitaries

$$U(B, \beta) = e^{-i\beta B} = \prod_{\nu=1}^n e^{-i\beta X_\nu}, \quad (5)$$

where $\beta \in [0, \pi)$ and B is the sum of all single-qubit Pauli-X operators

$$B = \sum_{\nu=1}^n X_\nu. \quad (6)$$

For any positive integer $p \geq 1$, the QAOA algorithm generates an angle-dependent quantum state using $2p$ angles, $\gamma = [\gamma_1, \gamma_2, \dots, \gamma_p]$ and $\beta = [\beta_1, \beta_2, \dots, \beta_p]$, where the subscripts of γ and β indicate the iterate number of the quantum ansatz. The quantum state has the form

$$|\gamma, \beta\rangle = U(B, \beta_p) U(C, \gamma_p) \cdots U(B, \beta_1) U(C, \gamma_1) |s\rangle, \quad (7)$$

where $|s\rangle$ denotes the uniform superposition over all n -bit strings

$$|s\rangle = \frac{1}{\sqrt{2^n}} \sum_{z \in \{0,1\}^n} |z\rangle. \quad (8)$$

We then compute the expectation value of C for the variational state described in eq. (7)

$$\langle C \rangle = \langle \gamma, \beta | C | \gamma, \beta \rangle, \quad (9)$$

which is accomplished by repeated measurements of fresh copies of the quantum system in the computational basis.

The optimal parameters (γ^*, β^*) that maximise the expectation value $\langle C \rangle$ are found using a classical computer:

$$(\gamma^*, \beta^*) = \arg \max_{\gamma, \beta} \langle C \rangle. \quad (10)$$

Typically, this is performed by estimating the parameters and then optimising them using simplex or gradient techniques. The approximation ratio r^* is a relevant metric for assessing the performance of QAOA, where

$$r^* = \frac{\langle C \rangle}{C_{\max}}. \quad (11)$$

We will focus on applying QAOA to the MaxCut problem for the rest of this paper. To this end, note that the optimisation problem in eq. (1) is equivalent to finding the maximum eigenvalue of the problem Hamiltonian C for MaxCut:

$$C = \sum_{\{u,v\} \in E} C_{uv}, \quad \text{with } C_{uv} = \frac{1}{2} w_{uv} (1 - Z_u Z_v), \quad (12)$$

where Z_i denotes the Pauli-Z matrix acting on the i -th qubit.

Before proceeding with the rest of the section, let us make a few definitions that will be used throughout the paper. For $w \in V$, let $\mathcal{N}(w) = \{x \in V : \{x, w\} \in E\}$ be the set of neighbours of w , i.e. vertices which are adjacent to w . Then, for an edge $\{u, v\} \in E$, we have that

- $e = \mathcal{N}(v) \setminus \{u\}$ is the set of vertices other than u that are connected to v .
- $d = \mathcal{N}(u) \setminus \{v\}$ is the set of vertices other than v that are connected to u .
- $F = \mathcal{N}(u) \cap \mathcal{N}(v)$ is the set of vertices that form a triangle with the edge $\{u, v\}$. In other words, F is the set of vertices that are neighbours of both u and v .

The following theorem can be used to compute the expectation value of the cost function for QAOA at $p = 1$ (QAOA₁) for MaxCut on arbitrary weighted graphs, thereby allowing us to assess the performance of QAOA₁.

Theorem 1. Consider the QAOA₁ state $|\gamma, \beta\rangle$ for MaxCut on an arbitrary weighted graph G . Then, the expectation value of C in $|\gamma, \beta\rangle$ is $\langle \gamma, \beta | C | \gamma, \beta \rangle = \sum_{\{u,v\} \in E} \langle C_{uv} \rangle$, where

$$\begin{aligned} \langle C_{uv} \rangle = & \frac{w_{uv}}{2} + \frac{w_{uv}}{4} \left[\sin 4\beta \sin \gamma'_{uv} \left(\prod_{w \in e} \cos \gamma'_{wv} + \prod_{w \in d} \cos \gamma'_{uw} \right) \right. \\ & \left. + \sin^2 2\beta \prod_{\substack{w \in e \\ w \notin F}} \cos \gamma'_{wv} \prod_{\substack{w \in d \\ w \notin F}} \cos \gamma'_{uw} \left(\prod_{f \in F} \cos(\gamma'_{uf} + \gamma'_{vf}) - \prod_{f \in F} \cos(\gamma'_{uf} - \gamma'_{vf}) \right) \right] \end{aligned} \quad (13)$$

and $\gamma'_{ij} = \gamma w_{ij}$.

In appendix D3, we give a proof of theorem 1, which we show follows as a straightforward corollary of our main theorem (theorem 3). By taking $w_{ij} = 1$ if $\{i, j\} \in E$ and 0 otherwise, eq. (13) simplifies for unweighted graphs to:

$$\langle C_{uv} \rangle = \frac{1}{2} + \frac{1}{4} \left\{ \sin 4\beta \sin \gamma (\cos^{|e|} \gamma + \cos^{|d|} \gamma) + \sin^2 2\beta \cos^{|e|+|d|-2|F|} \gamma (\cos^{|F|} 2\gamma - 1) \right\}, \quad (14)$$

which has previously appeared as eq. (14) of [80]⁴.

From theorem 1, we see that at $p = 1$, the expectation value $\langle C_{uv} \rangle$ of any edge in a graph depends on only the nodes and edges adjacent to it. The overall expectation value for QAOA₁ can then be calculated by summing the expectation values over all edges in the graph. For an n -node graph, the right-hand side of eq. (13) can be computed in linear time $O(n)$. Since the total number of edges in any graph is at most $\binom{n}{2} = O(n^2)$, computing the expectation value of QAOA would take at most $O(n^3)$ time. However, to find an actual bit string that represents an approximate solution for an arbitrary graph, here we use the QAOA quantum circuit to generate a quantum state on which measurement is performed.

C. Multi-Angle QAOA (MA-QAOA)

The Multi-Angle QAOA (MA-QAOA) [57] varies from the original QAOA in that it allows each summand of the problem and mixing Hamiltonians to have its own angle, as opposed to these Hamiltonians having a single angle each⁵. In this modification for $p = 1$ (called MA-QAOA₁), the problem and mixing unitaries are defined

as

$$U(\mathbf{C}, \boldsymbol{\gamma}) = e^{-i \sum_{\mu} \gamma_{\mu} C_{\mu}} = \prod_{\mu=1}^m e^{-i \gamma_{\mu} C_{\mu}}, \quad \text{and} \quad (15)$$

$$U(\mathbf{B}, \boldsymbol{\beta}) = e^{-i \sum_{\nu} \beta_{\nu} B_{\nu}} = \prod_{\nu=1}^n e^{-i \beta_{\nu} B_{\nu}}, \quad (16)$$

respectively, where $\mathbf{C} = (C_{\mu})_{\mu=1, \dots, m}$ and $\mathbf{B} = (B_{\nu})_{\nu=1, \dots, n}$ denote collections of operators. Thus, MA-QAOA₁ generates an angle-dependent quantum state of the form

$$|\boldsymbol{\gamma}, \boldsymbol{\beta}\rangle = U(\mathbf{B}, \boldsymbol{\beta}) U(\mathbf{C}, \boldsymbol{\gamma}) |s\rangle = \prod_{\nu=1}^n e^{-i \beta_{\nu} B_{\nu}} \prod_{\mu=1}^m e^{-i \gamma_{\mu} C_{\mu}} |s\rangle, \quad (17)$$

where $\boldsymbol{\gamma} = [\gamma_1, \gamma_2, \dots, \gamma_m]$ and $\boldsymbol{\beta} = [\beta_1, \beta_2, \dots, \beta_n]$. The subscript in γ_{μ} refers to the μ -th clause, and the subscript in β_{ν} refers to the ν -th qubit. In the context of MaxCut, μ and ν index the edges and vertices, respectively, of the graph involved. The approximation ratio obtained using QAOA lower bounds that of MA-QAOA, and MA-QAOA's guarantee of convergence to the exact solution as $p \rightarrow \infty$ follows immediately from [8, eq. (10)] and from noting that MA-QAOA is a generalisation of QAOA.

Herrman *et al.* [57] provide an analytical formula for computing the performance of MA-QAOA₁ on MaxCut for unweighted triangle-free graphs. We generalise their result with the following theorem, where we present an analytical formula for the expectation value of the cost function for MA-QAOA₁ for MaxCut on arbitrary weighted graphs, allowing for the assessment of MA-QAOA₁'s performance on general graphs.

Theorem 2. *Consider the MA-QAOA₁ state for MaxCut on an arbitrary graph G . Then, the expectation value of C in $|\boldsymbol{\gamma}, \boldsymbol{\beta}\rangle$ is $\langle \boldsymbol{\gamma}, \boldsymbol{\beta} | C | \boldsymbol{\gamma}, \boldsymbol{\beta} \rangle = \sum_{\{u,v\} \in E} \langle C_{uv} \rangle_{\text{MA}}$, where*

$$\begin{aligned} \langle C_{uv} \rangle_{\text{MA}} = & \frac{w_{uv}}{2} + \frac{w_{uv}}{2} \left[\cos 2\beta_u \sin 2\beta_v \sin \gamma'_{uv} \prod_{w \in e} \cos \gamma'_{wv} + \sin 2\beta_u \cos 2\beta_v \sin \gamma'_{uv} \prod_{w \in d} \cos \gamma'_{uw} \right. \\ & \left. + \frac{1}{2} \sin 2\beta_u \sin 2\beta_v \prod_{\substack{w \in e \\ w \notin F}} \cos \gamma'_{wv} \prod_{\substack{w \in d \\ w \notin F}} \cos \gamma'_{uw} \left(\prod_{f \in F} \cos(\gamma'_{uf} + \gamma'_{vf}) - \prod_{f \in F} \cos(\gamma'_{uf} - \gamma'_{vf}) \right) \right] \end{aligned} \quad (18)$$

⁴ One could also find similar analytical expressions for unweighted MaxCut in, for example, [81, eq. (5.10)]. See also [39, 82, 83], which provide analytical expressions for more general cost func-

tions.

⁵ Predating Herrman *et al.* [57] was earlier work by Farhi *et al.* [84], who first considered allowing for multiple angles in QAOA.

and $\gamma'_{jk} = \gamma_{jk} w_{jk}$.

We present, in appendix D 3, a proof of theorem 2, which again, is a straightforward corollary of our main theorem (theorem 3). Like eq. (13), the expectation value $\langle C_{uv} \rangle_{\text{MA}}$ for any edge in a graph depends on only its neighbouring nodes and edges, and the overall expectation value is the sum of the expectation values over all edges in the graph; hence, computing eq. (18) for an arbitrary graph has a time complexity of $O(n^3)$. However, this time complexity has a larger constant prefactor compared to that of computing eq. (13). While QAOA₁ involves only two hyperparameters regardless of the size of the problem, MA-QAOA₁ involves $|V| + |E| = O(n) + O(n^2)$ classical hyperparameters.

III. EXPRESSIVE QAOA (XQAOA)

The eXpressive QAOA builds on MA-QAOA by introducing an additional α -dependent unitary operator to the mixing Hamiltonian. Let us define the α -dependent operator to be the following product of commuting one-qubit operators:

$$U(\mathbf{A}, \boldsymbol{\alpha}) = e^{-i \sum_j \alpha_j A_j} = \prod_{j=1}^n e^{-i \alpha_j Y_j}, \quad (19)$$

where $\mathbf{A} = (A_i)_{i=1, \dots, n}$, and $\alpha \in [0, \pi]$ ⁶.

The mixing unitary is then given by the product of the $U(\mathbf{B}, \boldsymbol{\beta})$ and $U(\mathbf{A}, \boldsymbol{\alpha})$ unitary operators:

$$\begin{aligned} U(\mathbf{A}, \boldsymbol{\alpha}) U(\mathbf{B}, \boldsymbol{\beta}) &= e^{-i \sum_j \alpha_j A_j} e^{-i \sum_j \beta_j B_j} \\ &= \prod_{j=1}^n e^{-i \alpha_j Y_j} e^{-i \beta_j X_j}. \end{aligned} \quad (20)$$

Thus at $p = 1$, XQAOA generates an angle-dependent quantum state of the form

$$\begin{aligned} |\boldsymbol{\gamma}, \boldsymbol{\beta}, \boldsymbol{\alpha}\rangle &= U(\mathbf{A}, \boldsymbol{\alpha}) U(\mathbf{B}, \boldsymbol{\beta}) U(\mathbf{C}, \boldsymbol{\gamma}) |s\rangle \\ &= \prod_{j=1}^n e^{-i \alpha_j Y_j} e^{-i \beta_j X_j} \prod_{\mu=1}^m e^{-i \gamma_\mu C_\mu} |s\rangle, \end{aligned} \quad (21)$$

where $\boldsymbol{\alpha} = [\alpha_1, \alpha_2, \dots, \alpha_n]$, $\boldsymbol{\beta} = [\beta_1, \beta_2, \dots, \beta_n]$, and $\boldsymbol{\gamma} = [\gamma_1, \gamma_2, \dots, \gamma_m]$. Similarly to the eq. (17), the subscript in γ_i denotes the i -th clause, and the subscripts in α_i and

β_i refer to the i -th qubit, which in the context of MaxCut correspond to the edges and vertices, respectively, of the graph.

One motivation for introducing the XQAOA is that, unlike QAOA and MA-QAOA, the XY mixer⁷ in eq. (20) is the most general product (with respect to the n registers in the circuit) unitary operator one could write for $p = 1$ XQAOA, up to an unphysical global phase incurred when the system is measured immediately after the mixer unitary is applied. This makes XQAOA a natural generalisation of QAOA to consider, as one aims to maximise the expressiveness of the ansatz given the limitations on its depth, and also gives XQAOA the ability to output any computational-basis state given appropriate angles $\boldsymbol{\gamma}$, $\boldsymbol{\beta}$, and $\boldsymbol{\alpha}$. To see this, note that if we set the angles $\boldsymbol{\gamma} = \boldsymbol{\beta} = \mathbf{0}$ in (21), we are left with single-qubit Y-rotations on the $|+\rangle$ states. Choosing appropriate angles α_j on each qubit will bring $|+\rangle$ to $|0\rangle$ or $|1\rangle$. The same is true for when $\boldsymbol{\gamma} = \mathbf{0}$ and $\boldsymbol{\alpha} = \boldsymbol{\beta}$. Consequently, as we mentioned in section I, XQAOA is able to eschew any reachability deficits [44, 62].

Ansatz	No. of Parameters
MA-QAOA _p	$(n + m)p$
XQAOA _p ^{XY}	$(2n + m)p$
XQAOA _p ^Y	$(n + m)p$
XQAOA _p ^{X=Y}	$(n + m)p$

TABLE I: Summary of the XQAOA Ansatz family and the associated number of free parameters for p iterations of the ansatz for MaxCut on graphs with n vertices and m edges.

From eq. (21), it is clear that several variations of the XQAOA ansatz can be generated by placing restrictions on the allowed angles of the mixing unitaries. The MA-QAOA is a special case of the XQAOA ansatz obtained by setting all $\alpha_i = 0$. Other configurations of the XQAOA ansatz worth noting are those with the XY Mixer, Y Mixer, and the X=Y Mixer, respectively. The XY Mixer is the most general mixer and uses individual angles α_i , β_i for each unitary in the mixing Hamiltonian. The Y Mixer consists of only Pauli-Y gates and is obtained by setting all β_i to zero. The X=Y Mixer includes both Pauli-X and Pauli-Y gates but uses a single angle for both, with α_i equal to β_i .

As we summarise in table I, the XQAOA ansatzes with the XY mixer, Y mixer, and X=Y mixer for n qubits and m clauses require the classical optimisation of $2n +$

⁶ Due to the $\alpha \rightarrow \alpha + \pi$ and $\beta \rightarrow \beta + \pi$ translational symmetries of the QAOA output state, one could without loss of generality assume that α and β lie in the interval $[0, \pi)$. For the purposes of our simulations though, we do not place such an explicit restriction, since α and β repeat in intervals of π (in addition, for unweighted graphs, γ repeats in intervals of 2π) anyways. The data in fig. 5 were adjusted to fit the ranges mentioned in this paper.

⁷ The XY mixer used in XQAOA differs from Wang et al. [17]'s approach. We utilise a single-qubit mixer to increase the range of Hilbert Space explored for binary combinatorial optimisation, while Wang et al. employs a multi-qubit mixer in the Quantum Alternating Operator Ansatz to confine the search space to feasible solutions in integer-valued optimisation problems.

m , $n + m$, and $n + m$ angles, respectively. While the performances of these mixers are not known *a priori*, the XY mixer is expected to have a higher computational overhead than the other two mixers due to the presence of an additional n classical parameters. The X=Y mixer is expected to perform better than the Y mixer because it is able to trace a larger portion of the Bloch sphere due to its non-trivial trajectory, whereas the Y mixer is limited to the XZ plane.

In the remainder of the paper, we will use the superscript notation to indicate the specific variant of the XQAOA ansatz being used, i.e. $\text{XQAOA}_1^{\text{XY}}$,

$\text{XQAOA}_1^{\text{X=Y}}$, and $\text{XQAOA}_1^{\text{Y}}$ refer to $p = 1$ XQAOA with the XY, X=Y, and Y mixers, respectively. The next theorem—the main theorem of this paper—allows us to calculate the expectation value of the cost function for $\text{XQAOA}_1^{\text{XY}}$ for MaxCut on arbitrary weighted graphs, which in turn allows us to evaluate the performance of XQAOA.

Theorem 3. *Consider the $\text{XQAOA}_1^{\text{XY}}$ state $|\gamma, \beta, \alpha\rangle$ for MaxCut on an arbitrary weighted graph G . Then, the expectation value of C in $|\gamma, \beta, \alpha\rangle$ is $\langle \gamma, \beta, \alpha | C | \gamma, \beta, \alpha \rangle = \sum_{\{u,v\} \in E} \langle C_{uv} \rangle_{\text{XY}}$, where*

$$\begin{aligned} \langle C_{uv} \rangle_{\text{XY}} = & \frac{w_{uv}}{2} + \frac{w_{uv}}{2} \left[\cos 2\alpha_u \cos 2\alpha_v \sin \gamma'_{uv} \left(\cos 2\beta_u \sin 2\beta_v \prod_{w \in e} \cos \gamma'_{wv} + \sin 2\beta_u \cos 2\beta_v \prod_{w \in d} \cos \gamma'_{uw} \right) \right. \\ & - \frac{1}{2} \sin 2\alpha_u \sin 2\alpha_v \prod_{\substack{w \in e \\ w \notin F}} \cos \gamma'_{wv} \prod_{\substack{w \in d \\ w \notin F}} \cos \gamma'_{uw} \left(\prod_{f \in F} \cos(\gamma'_{uf} + \gamma'_{vf}) + \prod_{f \in F} \cos(\gamma'_{uf} - \gamma'_{vf}) \right) \\ & \left. + \frac{1}{2} \cos 2\alpha_u \sin 2\beta_u \cos 2\alpha_v \sin 2\beta_v \prod_{\substack{w \in e \\ w \notin F}} \cos \gamma'_{wv} \prod_{\substack{w \in d \\ w \notin F}} \cos \gamma'_{uw} \left(\prod_{f \in F} \cos(\gamma'_{uf} + \gamma'_{vf}) - \prod_{f \in F} \cos(\gamma'_{uf} - \gamma'_{vf}) \right) \right] \end{aligned} \quad (22)$$

and $\gamma'_{jk} = \gamma_{jk} w_{jk}$.

We present a proof of theorem 3 in appendix D 2. Like eq. (13) and eq. (18), the expectation value of any edge in a graph $\langle C_{uv} \rangle_{\text{XY}}$ is determined by its neighbouring nodes and edges, and the overall expectation value is the sum of the expectation values of all edges in the graph. Calculating eq. (22) for an arbitrary graph also has a time complexity of $O(n^3)$, but has a larger prefactor compared to both eq. (13) and eq. (18). While QAOA₁ requires only two parameters regardless of the problem size and MA-QAOA₁ requires $n + n^2$ parameters, $\text{XQAOA}_1^{\text{XY}}$ requires $2n + n^2$ parameters. In contrast, both $\text{XQAOA}_1^{\text{Y}}$ and $\text{XQAOA}_1^{\text{X=Y}}$ require $n + n^2$ parameters.

In the following corollary, we show that for unweighted graphs with edges of odd edge degrees, the $\text{XQAOA}_1^{\text{Y}}$ ansatz can solve MaxCut exactly. Here, the edge degree $d(e)$ of an edge $e = \{u, v\} \in E$ is defined as the number of neighbours of e , i.e., $d(e) = |\mathcal{N}(u) \cup \mathcal{N}(v)| - 2$.

Corollary 4. *Consider an unweighted graph G where the edge degree of every edge is odd. Then, when $\gamma = \pi$ and $\alpha = \frac{\pi}{4}$, the $\text{XQAOA}_1^{\text{Y}}$ state $|\gamma, \alpha\rangle$ provides the exact MaxCut solution for G , where $|\gamma, \alpha\rangle$ denotes the state in eq. (21) where all $\gamma_i = \gamma$, $\beta_i = 0$, and $\alpha_i = \alpha$.*

We give a proof of corollary 4 in appendix D 4. One consequence of corollary 4 is that it allows us to identify a graph instance for which we can analytically prove a

separation between $\text{XQAOA}_1^{\text{Y}}$ and QAOA₁. Our next corollary elucidates this result.

Corollary 5. *For the unweighted 5-vertex star graph G , $\text{XQAOA}_1^{\text{Y}}$ with optimal angles (say, from corollary 4) computes the MaxCut of G with an expected (and worst-case) approximation ratio of 1, whereas the expected approximation ratio of QAOA₁ with optimal angles is only 0.75.*

We give a proof of corollary 5 in appendix D 5. While our result above pertains to the 5-vertex star graph (see fig. 2), one can readily generalise this proof to any t -vertex star graph, where $t \geq 5$ is odd (here, the oddness criterion arises because it is only for odd-vertex star graphs that the edge degrees of the graph are all odd). The statement that QAOA₁ achieves an optimal expected approximation ratio of 3/4 for these graphs could be considered a finite-dimensional analogue of [57, Section IV]'s result that in the limit as the number of vertices tends to infinity, the performance of QAOA₁ approaches 0.75 for star graphs. In terms of the expected approximation ratio that can be achieved, this infinite class of graphs instantiates a clear advantage that XQAOA has over QAOA.

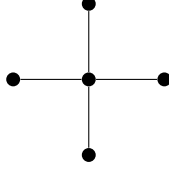


FIG. 2: Diagrammatic representation of the 5-vertex star graph S_4 , which we use to show an advantage that XQAOA has over QAOA. More specifically, we show that while XQAOA_1^Y can find the MaxCut of S_4 with an approximation ratio of 1, QAOA_1 can achieve an approximation ratio of at most $3/4$.

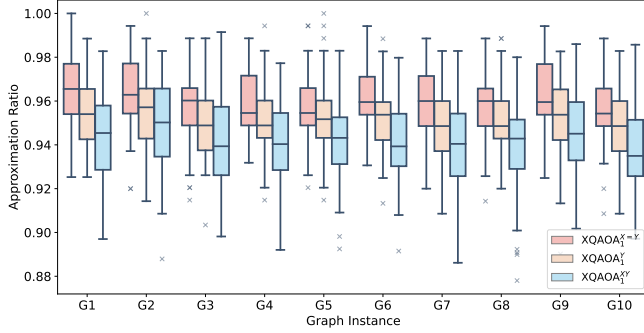


FIG. 3: Improvement of $\text{XQAOA}_1^{X=Y}$ ansatz over the XQAOA_1^{XY} and XQAOA_1^Y ansatz for ten different instances of 3-regular graphs with 128 vertices. For each of the three ansatz variants, the Parallel-LBFGS optimiser was run 100 times with random initial values for each of the ten graph instances.

IV. COMPUTATIONAL RESULTS

We evaluate the performance of the XQAOA algorithm by benchmarking it on the MaxCut problem on unweighted D -regular graphs that were generated using an algorithm developed by Steger and Wormald [85]. Since the three different configurations XQAOA_1^{XY} , $\text{XQAOA}_1^{X=Y}$ and XQAOA_1^Y of XQAOA that we consider have performances that are not known *a priori*, we first benchmark them on 10 randomly generated instances of 3-regular graphs with 128 vertices. The best-performing configuration of XQAOA_1 is then benchmarked against MA-QAOA_1 , QAOA_1 , and the CR and GW algorithms on 25 instances of D -regular graphs with 128 and 256 vertices for $3 \leq D \leq 10$. The XQAOA_1 , MA-QAOA_1 , QAOA_1 , and CR algorithms are benchmarked by performing 100 runs of the classical optimiser with random initial points, whereas the GW algorithm is benchmarked by first solving the relaxed problem and then generating 100 random vectors for hyperplane rounding. For an explanation of the GW algorithm, we refer the reader to appendix A. The CR algorithm computes the MaxCut by simply running the optimiser on the relaxed version

of eq. (1), i.e.

$$\text{Maximise} \quad \sum_{\{u,v\} \in E} \frac{1}{2} w_{uv} (1 - \sin \theta_u \sin \theta_v), \quad (23)$$

where the maximisation is performed over angles θ_u and θ_v .

To compute the approximation ratio, we need to obtain the exact MaxCut values, which we did using the GUROBI solver [86], a widely used industry tool. Although proving optimality with GUROBI takes exponential time, it can find solutions quickly. GUROBI was able to identify optimal solutions for 128-node graphs and near-optimal solutions for 256-node graphs with at most 6% MIPGap⁸. To compute the expectation values of QAOA_1 , MA-QAOA_1 , and XQAOA_1 for large n , we used the analytical results from theorems 1, 2, and 3. The Parallel-LBFGS algorithm was used to optimise the variational parameters of QAOA_1 , MA-QAOA_1 , XQAOA_1 , and the CR algorithm.

Finally, to assess the performance of quantum algorithms at increased depths, we expanded our benchmarking to include depths ranging from 1 to 5 for the most effective XQAOA variant, as well as QAOA and MA-QAOA . Due to the lack of analytical formulas for larger p values and the significant computational complexity associated with simulating deep quantum circuits, we conducted our benchmarks using the Qiskit [87] simulator on small graphs.

A. Benchmark Results for $p = 1$

Our comparative analysis of the three XQAOA variants on 3-regular graphs revealed that the $\text{XQAOA}_1^{X=Y}$ variant performed the best (see fig. 3). When benchmarked against MA-QAOA_1 , QAOA_1 , CR, and the GW algorithm on D -regular graphs with 128 and 256 vertices for $3 \leq D \leq 10$, $\text{XQAOA}_1^{X=Y}$ consistently outperformed QAOA_1 , MA-QAOA_1 , and the CR algorithm on all graph instances. Notably, $\text{XQAOA}_1^{X=Y}$ demonstrated competitive performance against the GW algorithm for 3 and 4-regular graphs and exceeded it for D -regular graphs with $D > 4$ (see fig. 4⁹). The boxplots reveal that the

⁸ The MIPGap is the gap between the lower and upper objective bound divided by the absolute value of the incumbent objective value.

⁹ Here, we note that in fig. 4, the boxplots for the $\text{XQAOA}_1^{X=Y}$, CR, and GW algorithms show the distributions of the approximation ratios obtained for individual solutions. Notably, for $\text{XQAOA}_1^{X=Y}$, individual solutions were classically extracted by leveraging the quantum-classical transition, a phenomenon detailed in section IV B. In contrast, the boxplots for QAOA_1 , QAOA_1^* , and MA-QAOA_1 show the distributions of expected approximation ratios; we do this in lieu of computing the approximation ratios of individual solutions, as the latter would require implementation of the quantum algorithm on a quantum

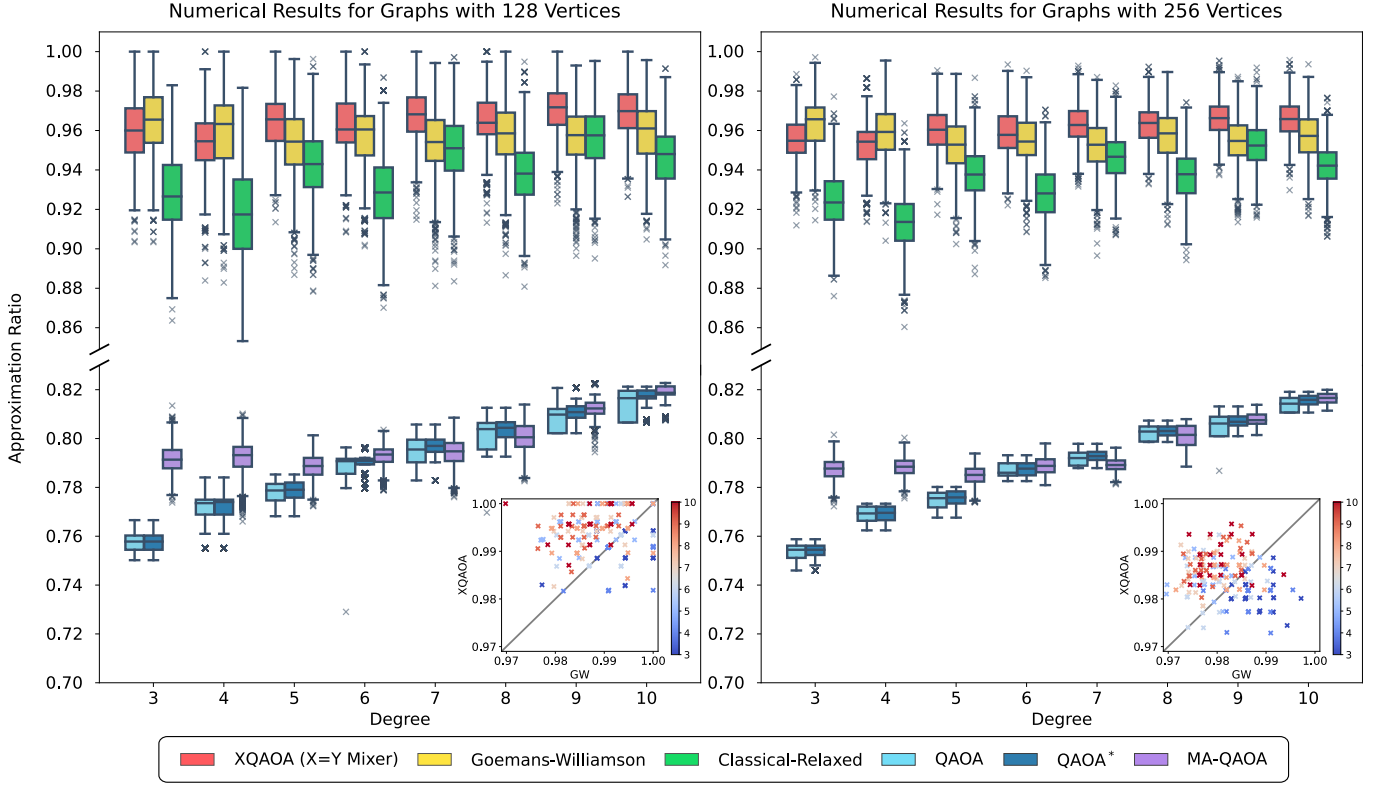


FIG. 4: This boxplot compares the sizes of cuts obtained by quantum and classical algorithms against the maximum cut size found by GUROBI. The data used to create the boxplots comes from 100 random cuts generated using the GW algorithm, 100 random initialisations for several other algorithms ($XQAOA_1^{X=Y}$, $MA-QAOA_1$, $QAOA_1$, and CR), and 100 informed initialisations for $QAOA_1$ (labelled as $QAOA^*$) applied to 25 different instances of regular graphs with 128 or 256 nodes and degree values ranging from 3 to 10. The whiskers extend up to data points within 1.5 times the interquartile range from the upper and lower quartiles, and crosses represent outliers. For clarity, outliers of $QAOA_1$, with approximation ratios less than 0.7, that resulted from the barren plateau have been omitted. The inset scatterplot compares the best-found solutions for 100 runs for the $XQAOA_1^{X=Y}$ and the GW algorithm on all the graph instances. The points in the upper-left corner show that $XQAOA_1^{X=Y}$ performs better than GW, while the opposite is true for points in the lower-right corner. The colour of the points indicates the degree of the corresponding graph.

lower, middle and upper quartile values of $XQAOA_1^{X=Y}$ are significantly higher than those of the GW algorithm for graphs with $D > 4$, indicating that $XQAOA_1^{X=Y}$ is more likely to produce a better solution irrespective of the parameter initialisation strategy. This robustness of the $XQAOA_1^{X=Y}$ to initial parameter choices can be attributed to its overparameterised ansatz, which is further explained in section V C.

Our analysis also highlighted a linear increase in the approximation ratio of $QAOA_1$ with the degree of the

graph. Its performance nears that of $MA-QAOA_1$ for $D > 5$, hinting at a possible reachability deficit [44, 62], limiting $MA-QAOA_1$'s ability to find an approximate solution close to the optimal. It is also important to note that the $QAOA_1$ ansatz experiences the barren plateau phenomenon [89], with the size of the plateau increasing with the degree of the graph. To mitigate this, careful selection of initial points for the classical optimiser is crucial, as outlined in appendix C. The results of this strategy are also presented in fig. 4 as $QAOA^*$.

computer in order to obtain samples from measuring the output states of the circuits involved. Hence, the actual solutions obtained from $QAOA_1$, $QAOA^*$, and $MA-QAOA_1$ may differ from the expected approximation ratios shown in the boxplots, and could be either higher or lower. For an extended discussion of the distinction between using expected approximation ratios and approximation ratios of individual samples, we refer the reader to Larkin *et al.* [88].

B. Quantum-Classical Transition

In our numerical simulations with the $XQAOA_1^{X=Y}$ ansatz, we observed that as the classical optimiser converged to an optimum, the optimal angles (γ^*, β^*) stabilised at specific values. Specifically, γ_{uv}^* converged to

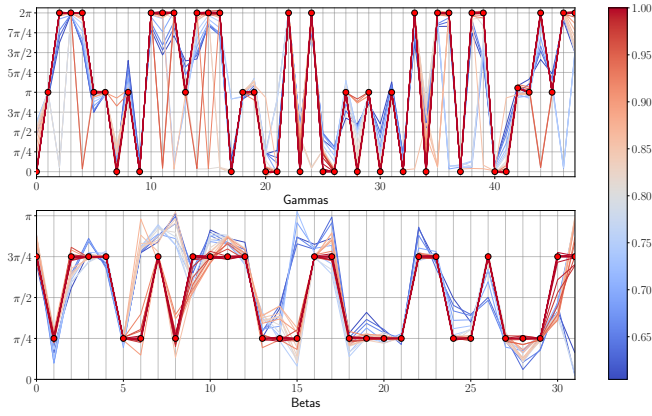


FIG. 5: This graph illustrates the changes in the γ and β angles of the $\text{XQAOA}_1^{X=Y}$ ansatz as the classical optimiser reaches the optimal solution for a 3-regular graph with 32 vertices and 48 edges. Each line in the graph represents a set of evaluated parameters, with the colour indicating the corresponding approximation ratio. The solid red circles in the graph represent the final angles determined by the classical optimiser for the $\text{XQAOA}_1^{X=Y}$ ansatz.

values in $\{0, \pi, 2\pi\}$ ¹⁰, while β_u^* converged to values in $\{\pi/4, 3\pi/4\}$ (see fig. 5). When $\gamma_{uv}^* \in \{0, 2\pi\}$, the two-qubit $\text{RZZ}(0)$ and $\text{RZZ}(2\pi)$ gates act as the identity gate, leaving qubits u and v unchanged. When $\gamma_{uv}^* = \pi$, the two-qubit gate $\text{RZZ}(\pi) = |+, +\rangle\langle -, -| + |-, -\rangle\langle +, +|$. In other words, it swaps the states $|+\rangle_u \leftrightarrow |-\rangle_u$ and $|+\rangle_v \leftrightarrow |-\rangle_v$. Since the initial state $|s\rangle$ is a product state $|+\dots+\rangle$, the state after all two-qubit gates will be a product state of $|+\rangle$ s and $|-\rangle$ s. Specifically, qubit u will be in the $|+\rangle_u$ state if it is swapped an even number of times and in the $|-\rangle_u$ state if it is swapped an odd number of times. Finally, the action of the mixing gates is to convert the $|+\rangle$ and $|-\rangle$ states to $|0\rangle$ or $|1\rangle$ depending on the value of β^* :

$$\text{When } \beta_i^* = \pi/4, \begin{cases} |+\rangle_i \rightarrow |1\rangle_i \\ |-\rangle_i \rightarrow |0\rangle_i \end{cases} \quad (24)$$

$$\text{and when } \beta_i^* = 3\pi/4, \begin{cases} |+\rangle_i \rightarrow |0\rangle_i \\ |-\rangle_i \rightarrow |1\rangle_i \end{cases}, \quad (25)$$

allowing us to read off the classical bit-string. It is important to acknowledge that due to degenerate local optimums, a relatively small subset of angles might not stabilise at the specified values even after convergence. Given the benign characteristics of the $\text{XQAOA}_1^{X=Y}$ ansatz's loss landscape, such deviations are highly un-

likely. However, in cases where deviations occur, we force γ_{uv}^* to take the closest value in $\{0, \pi, 2\pi\}$ ¹¹.

Reviewing fig. 5 from a different perspective, we observe that the $\text{XQAOA}_1^{X=Y}$ ansatz, initially set with random angles, creates a highly entangled quantum state with a multitude of superposed states. As optimisation progresses, this entanglement gradually decreases, leading to a marked reduction in the number of superposed states. When the optimum is reached, the entangling layer disappears, leaving the system in a singular definitive state. In essence, what begins as a distinctly quantum state, through the course of optimisation, evolves into a classical state. This transition, marked by the disappearance of the entangling layer, facilitates the extraction of the solution through classical means, negating the need for quantum computers. This quantum-to-classical transition raises a natural question of whether the entangling layer is fundamentally necessary. To answer this,

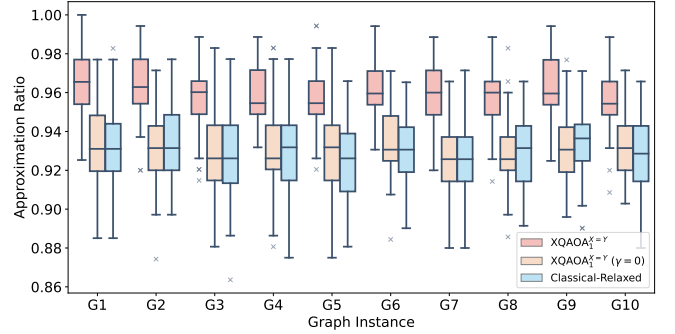


FIG. 6: Improvement of $\text{XQAOA}_1^{X=Y}$ ansatz over $\text{XQAOA}_1^{X=Y}$ with $\gamma = 0$, and the Classical-Relaxed algorithms for ten different instances of 3-regular graphs with 128 vertices. For each of the three ansatz variants, the Parallel-LBFGS optimiser was run 100 times with random initial values for each of the ten graph instances.

we conducted further numerical simulations by setting $\gamma = \mathbf{0}$ and optimising only the β angles. Our numerical results showed that without any entangling layer, the performance of $\text{XQAOA}_1^{X=Y}$ was similar to that of CR (see fig. 6). In fact, when we set $\gamma = \mathbf{0}$, eq. (22) reduces to

$$\langle C_{uv} \rangle_{X=Y} = \frac{1}{2} w_{uv} (1 - \sin 2\beta_u \sin 2\beta_v), \quad (26)$$

which is the same as eq. (23) with the angles having an additional factor of 2. This demonstrates that the over-parameterised entangling layer augments the landscape, making the gradient-based classical optimiser less susceptible to getting trapped in local optima.

¹⁰ In weighted graphs, the optimal angles γ_{uv}^* are scaled by the edge weight w_{uv} . The effective optimal angle, discounting the weight prefactor, can be calculated as $\gamma_{uv}^* = w_{uv} \gamma_{uv}^* \bmod 2\pi$.

¹¹ For example, in a two-vertex graph, if $\gamma_{uv}^* \notin \{0, \pi, 2\pi\}$, the final state may be entangled, such as $c_0 |01\rangle + c_1 |10\rangle$. In this scenario, both measurement outcomes '01' and '10' yield the same MaxCut value, rendering the specific choice of γ_{uv}^* inconsequential.

C. Benchmark Results for $1 \leq p \leq 5$

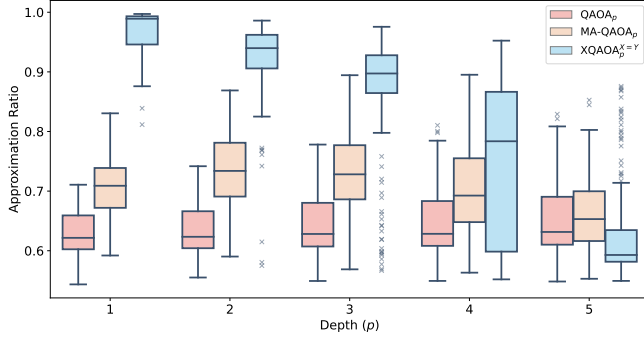


FIG. 7: Comparison of approximation ratios achieved by QAOA_p , MA-QAOA_p , and $\text{XQAOA}_p^{X=Y}$ for $1 \leq p \leq 5$, evaluated across 20 instances of 3-regular graphs, each with 16 vertices. The Powell optimiser was run 10 times with random initialisation for each graph instance across all three algorithms.

In previous sections, we showed that $\text{XQAOA}_1^{X=Y}$ achieves near-optimal solutions and surpasses QAOA_1 and MA-QAOA_1 . This led us to compare $\text{XQAOA}_p^{X=Y}$'s performance with QAOA_p and MA-QAOA_p for $p > 1$. Lacking analytical formulas for expectation values for $p > 1$ and constrained by the computational overhead of large-scale quantum simulation, we performed small-scale simulations using Qiskit [87], benchmarking 20 random 3-regular graph instances with 16 vertices each. Given the variability in expectation values due to the limited number of shots (1024), we utilised the Powell optimiser [90] with ten random restarts to optimise the ansatzes' parameters. The simulation results, presented in fig. 7, reveal that the median approximation ratio of $\text{XQAOA}_p^{X=Y}$ consistently outperforms QAOA_p and MA-QAOA_p up to $p = 4$, with $\text{XQAOA}_1^{X=Y}$'s median nearly reaching 1.0. Interestingly, while QAOA_p shows modest improvement with increasing depth, MA-QAOA_p peaks at $p = 3$ before declining at $p \geq 4$ ¹². In contrast, $\text{XQAOA}_p^{X=Y}$ exhibits a gradual decline in performance beyond $p = 1$, particularly noticeable at $p \geq 4$. This decline is attributed to barren plateaus due to the circuit's overexpressiveness, rather than a lack of effectiveness at higher depths [92, 93].

¹² It should be noted that MA-QAOA_p 's performance is lower-bounded by QAOA_p when its parameter optimisation is warm-started with the optimal angles of QAOA_p . The suboptimal results of MA-QAOA_p in our simulations stem from the use of random parameter initialisation. For a detailed analysis of $\text{MA-QAOA}_{p>1}$'s performance with various parameter initialisation strategies, see Gaidai *et al.*[91].

V. DISCUSSION

A. Randomness in the Approximation Algorithms

We optimise the classical parameters of XQAOA_1 , MA-QAOA_1 , QAOA_1 , and CR algorithms using a gradient-based classical optimiser. We start the optimisation process with a randomly chosen initial point which affects the quality of the solution found, especially if the optimisation landscape is non-convex and has non-trivial features. If the initial point is near a local optimum or barren plateau, the gradient-based optimiser will converge to the local optimum and return a suboptimal solution. As a result, XQAOA_1 , MA-QAOA_1 , QAOA_1 , and CR algorithms have a wide range of approximate solutions for the same problem. The maximum approximation ratio returned by MA-QAOA_1 is 0.82, whereas XQAOA_1 can often achieve an approximation ratio of 1.0 with the right choice of initial parameters. The range of approximation ratios for the CR algorithm is similar to XQAOA_1 , but numerical simulations suggest that the cost landscape of the CR algorithm may be difficult to navigate and plagued with local optima, which may require an exponential number of initial points for the CR to match XQAOA_1 's performance, thus negating the benefit of having a polynomial-time approximation algorithm.

The GW algorithm also has randomness in its process. After it solves the relaxed version of the MaxCut problem, it generates an n -dimensional random vector \mathbf{r} to perform its hyperplane rounding to find the optimal cut. While GW has an expected approximation ratio of 0.87856 in the worst case at the asymptotic limit, the distribution of the approximation ratio returned by the GW algorithm for a finite number of randomly generated \mathbf{r} vectors and problem instances can vary significantly, which is why we see a distribution for the output of the GW algorithm. While XQAOA_1 , MA-QAOA_1 , and the CR algorithm each require solving the problem anew for each random initial point, the GW algorithm solves the relaxed MaxCut problem just once and then efficiently generates individual solutions through hyperplane rounding with randomly generated vectors, avoiding repetitive computations.

B. Classical Simulability of the XQAOA Ansatz

Computing expectation values of QAOA_1 , MA-QAOA_1 , and XQAOA_1 for MaxCut on arbitrary graphs all have a time complexity of $O(n^3)$, albeit with varying prefactors. XQAOA_1 is unique in that its entangling layer vanishes at the optimal solution, in contrast to QAOA_1 and MA-QAOA_1 , which maintain their entangling layer post-convergence. This entangling layer in QAOA_1 and MA-QAOA_1 requires generating an entangled quantum state through quantum computation followed by measurements to assign values to variables,

precluding efficient classical simulation. In contrast, XQAOA_1 's optimal state, characterised by zero gammas, is non-entangled and permits classical bit assignment without quantum computation. However, in cases where XQAOA_1 falls short, a $p > 1$ XQAOA_p might be required, necessitating quantum computation.

It remains an open question whether a simple analytical formula exists for efficiently computing the mean values of Pauli operators of the XQAOA_1 , MA-QAOA_1 , and QAOA_1 states when dealing with k -local Ising Hamiltonians for $k > 2$. Additionally, if the problem assignments take integer-valued arguments, the quantum circuit would require more qubits per variable, further increasing the entangling and non-locality of the circuit, potentially allowing for quantum advantage. The $p = 1$ Recursive QAOA (RQAOA_1) [39] is another quantum algorithm that can solve the MaxCut problem classically in time $O(n^4)$ without requiring any quantum computation or multi-qubit measurements.

C. Role of Overparameterisation in XQAOA

The efficacy of XQAOA largely stems from its overparameterised ansatz. Overparameterisation, which involves introducing additional parameters to increase model dimensionality, reshapes the loss landscape to facilitate easier optimisation. To understand the impact of overparameterisation, consider the role of local minima in this context: a local minimum is a point in the loss landscape with a loss value lower or equal to those of its neighbours within an ϵ radius. While such minima are prevalent in lower dimensions, they become less likely with increasing dimensionality as it becomes harder for their loss values to remain the lowest across all new dimensions, converting them from minima into saddle points. Saddle points differ from local minima as they are not the lowest points in all directions; thus, optimisers can navigate past them more readily. As overparameterisation turns more potential local minima into saddle points, the path to the global minimum becomes less obstructed. Although the overparameterised models may not be completely devoid of local minima, the remaining local minima tend to be close to the global minimum. This proximity reduces the likelihood of settling for sub-optimal solutions and facilitates more efficient convergence to the global minimum [94–98]. This advantageous effect of overparameterisation is evident in fig. 4, where the lower quartiles for $\text{XQAOA}_1^{X=Y}$ consistently surpass 0.92 approximation ratio on all the benchmarked graph instances, strongly hinting at the benign loss landscape devoid of barren plateaus and suboptimal local minima.

While the previous discussion intuitively explains how overparameterisation enhances the efficacy of XQAOA , it's crucial to place this within the wider context of ongo-

ing research on the trainability¹³ of parameterised quantum circuits (PQCs). These studies, which form the basis of quantum landscape theory (QLT) [99], offer a deeper understanding of quantum loss landscapes [37, 48, 53, 89, 92, 93, 100–106]. QLT defines a PQC to be overparameterised when it has sufficiently many parameters to explore all relevant directions of its state space [99]. An essential aspect of this definition is the inherent expressiveness of the PQC, which is characterised by its ability to generate a wide range of unitaries under varied parameter settings [107]. This distinction is particularly evident when comparing $\text{XQAOA}_1^{X=Y}$ and MA-QAOA_1 for the MaxCut problem; despite having an equal number of parameters, $\text{XQAOA}_1^{X=Y}$ consistently outperforms MA-QAOA_1 on all problem instances. However, high expressivity also has drawbacks, such as the barren plateau phenomenon, where circuits show vanishingly small gradients due to their expressiveness [92]. XQAOA addresses this by using a problem-specific ansatz, tailoring its circuit design to the task at hand. This approach allows XQAOA to be overparameterised with a quadratic number of parameters, in contrast to generic ansatzes that may require exponentially more parameters and deeper circuits [99, 108]. XQAOA thus achieves an optimal balance, avoiding both the limitations of underparameterisation, such as spurious local minima and reachability deficits [53], and the challenges of high expressivity like barren plateaus. This positions XQAOA in an optimal ‘Goldilocks zone’ of trainability and expressivity.

D. Shallow XQAOA vs Deep QAOA

The decision to use shallow XQAOA versus deep QAOA circuits hinges on their trainability for a given problem. Trainability depends on the loss landscapes of their ansatzes, influenced by factors like parameter count, initialisation strategy, circuit depth, and hardware noise. These factors can adversely affect trainability, hindering optimisation. Thus, the choice between shallow XQAOA and deep QAOA is determined by their relative trainability under these conditions.

It is evident that to surpass the performance of XQAOA_1 , QAOA circuits need to be sufficiently deep. For example, it is conjectured that a minimum depth of $p = 12$ is necessary for QAOA to outperform the GW algorithm on the MaxCut problem on unweighted 3-regular graphs [43]. This conjecture not only posits a depth requirement but also suggests a parameter ini-

¹³ In this context, ‘trainability’ refers to the ability of a PQC to efficiently adjust its variational parameters for optimising a cost function. The terms ‘train,’ ‘trainable,’ and ‘trainability’ are often used interchangeably with ‘optimise’ and ‘optimisable’ in quantum algorithms literature due to the parallel drawn between PQCs and Quantum Neural Networks, where the process of optimising network variables is commonly referred to as ‘training.’

tialisation strategy of using a set of predetermined angles for warm-starting the optimisation. However, this strategy becomes ineffective in the presence of hardware noise [48]. The noise distorts the loss landscape, leading to barren plateaus, and necessitates deeper, more noise-prone circuits. In contrast, our findings suggest that $\text{XQAOA}_1^{X=Y}$ is adequate for the MaxCut problem, questioning the need for deeper XQAOA circuits on NISQ devices. While XQAOA may require $p > 1$ for certain problems, necessitating quantum computation, its relatively shallower depth compared to QAOA makes it less susceptible to noise. With sufficiently low noise levels, XQAOA can still achieve near-optimal solutions, albeit with additional random restarts or parameter initialisation strategies [105].

For problems unlike MaxCut on unweighted 3-regular graphs, where patterns are ambiguous [37, 106] and *a priori* information is limited, training deep QAOA circuits is more challenging [109]. This is due to the difficulty in determining the minimal effective depth [110] and suitable parameter initialisation strategies in scenarios where random initialisation is suboptimal [89]. For such problems, where extracting useful *a priori* information is challenging, XQAOA may be a preferable choice, regardless of whether the quantum computers are NISQ or fault-tolerant. An example of such a problem could be the MaxCut on randomly weighted regular graphs or randomly generated graphs.

VI. CONCLUSION

In this work, we presented the XQAOA ansatz and its variants and explained how they generalise the MA-QAOA and QAOA ansatzes. Our numerical simulations reveal that a single iteration of the XQAOA ansatz, especially with the $X=Y$ mixer, outperforms a single iteration of both MA-QAOA and QAOA. This enhanced performance of XQAOA is attributed to its overparameterised ansatz, which enables exploration in all relevant directions of its state space. The incorporation of the Pauli-Y rotation gate also significantly contributes to this improved efficacy. Our benchmarks also reveal that XQAOA performs just as well as the state-of-the-art Goemans-Williamson algorithm and even outperforms it for unweighted regular graphs with degrees greater than 4. Additionally, we find that the naive Classical-Relaxed algorithm with fewer classical parameters than MA-QAOA performs better by a large margin and that the performance of QAOA grows arbitrarily close to MA-QAOA for regular graphs with increasing degrees. Finally, we find an infinite family of graphs for which XQAOA solves MaxCut exactly and show analytically that for some graphs in this family, special cases of XQAOA are capable of achieving a much larger approximation ratio than QAOA.

Interestingly, we found that as the $\text{XQAOA}_1^{X=Y}$ ansatz converges to an optimum, its entangling layer disap-

pears, leaving behind only single-qubit unitaries, making it possible to efficiently solve and extract the solution classically. Although the entangling layer disappears as the ansatz reaches an optimal solution, it is necessary for the optimisation process, without which the performance of the $\text{XQAOA}_1^{X=Y}$ ansatz deteriorates to that of the Classical-Relaxed algorithm. Although for the problem of MaxCut, the efficient classical simulation of the $p = 1$ XQAOA ansatz eliminates quantum advantage, it remains open whether this is still the case for larger p and problems whose Ising formulations are 2-local with external fields or k -local with $k > 2$.

We have also shown that despite the XQAOA ansatz being overparameterised—with a quadratic increase in free parameters in the worst-case scenario—it is significantly easier to train compared to the underparameterised QAOA ansatz and the adequately parameterised Classical-Relaxed algorithm. The QAOA ansatz struggles with issues like spurious local minima, barren plateaus, and reachability deficits, while the Classical-Relaxed algorithm often encounters sub-optimal local minima far from the global optimum. In contrast, the XQAOA ansatz, like other overparameterised models, features a more benign loss landscape, free from barren plateaus, spurious local minima, and reachability deficits. This characteristic enables the classical optimiser to consistently converge to optimal or near-optimal solutions, independent of the parameter initialisation strategy. While the increased number of free parameters in XQAOA might suggest higher computational costs, its faster convergence rate, eliminating the need for specific initialisation strategies or random restarts, compensate for the extra parameters’ computational overhead.

Our work opens up new avenues for further research into improving quantum optimisation algorithms as well as their impact on various applications. For example, QAOA and its variants have already found numerous potential uses in solving various optimisation problems beyond MaxCut, including problems in graph theory [111–113], finance [114], chemistry [115, 116], and others [15, 117]. Future work could extend these results by adopting and exploiting the advantages of XQAOA in various applications. In addition, due to its advantages at low depth, XQAOA could be tested and implemented on near-term quantum hardware and compared against existing experimental benchmarks [112, 117–119].

VII. ACKNOWLEDGEMENTS

VV is thankful to Ye Jun from the A*STAR Institute of High Performance Computing and the A*STAR Computational Resource Centre for supporting this work through the use of their high-performance computing facilities. VV is thankful to Aaron Tranter for the stimulating discussions and insightful suggestions. We thank Truman Ng for helpful comments on an earlier version of this manuscript. This research is supported by A*STAR

C230917003 and the Australian Research Council Centre of Excellence CE170100012. DEK acknowledges funding support from the A*STAR Central Research Fund (CRF) Award for Use-Inspired Basic Research; and the National Research Foundation, Singapore and A*STAR under the Quantum Engineering Programme (NRF2021-QEP2-02-P03).

VIII. DATA AVAILABILITY

We provide a total of 420 D -regular graphs that were used in this paper, along with their optimal cut and their

solutions in a machine-readable CSV format. We also provide the simulation data and scripts used to generate the plots presented in this paper. The benchmark and simulation dataset and the scripts for generating the plots can be found at <https://github.com/vijeycreative/XQAOA-Dataset> [120].

-
- [1] M. E. Beverland, P. Murali, M. Troyer, K. M. Svore, T. Hoefler, V. Kliuchnikov, G. H. Low, M. Soeken, A. Sundaram, and A. Vasilchillo, Assessing requirements to scale to practical quantum advantage, *arXiv preprint arXiv:2211.07629* (2022).
 - [2] J. Preskill, Quantum Computing in the NISQ era and beyond, *Quantum* **2**, 79 (2018).
 - [3] J. W. Z. Lau, K. H. Lim, H. Shrotriya, and L. C. Kwek, NISQ computing: where are we and where do we go?, *AAPPS Bulletin* **32**, 27 (2022).
 - [4] M. Cerezo, A. Arrasmith, R. Babbush, S. C. Benjamin, S. Endo, K. Fujii, J. R. McClean, K. Mitarai, X. Yuan, L. Cincio, *et al.*, Variational quantum algorithms, *Nature Reviews Physics* **3**, 625 (2021).
 - [5] K. Bharti, A. Cervera-Lierta, T. H. Kyaw, T. Haug, S. Alperin-Lea, A. Anand, M. Degroote, H. Heimonen, J. S. Kottmann, T. Menke, W.-K. Mok, S. Sim, L.-C. Kwek, and A. Aspuru-Guzik, Noisy intermediate-scale quantum algorithms, *Rev. Mod. Phys.* **94**, 015004 (2022).
 - [6] J. Tilly, H. Chen, S. Cao, D. Picozzi, K. Setia, Y. Li, E. Grant, L. Wossnig, I. Rungger, G. H. Booth, and J. Tennyson, The variational quantum eigensolver: A review of methods and best practices, *Physics Reports* **986**, 1 (2022).
 - [7] A. Peruzzo, J. McClean, P. Shadbolt, M.-H. Yung, X.-Q. Zhou, P. J. Love, A. Aspuru-Guzik, and J. L. O’Brien, A variational eigenvalue solver on a photonic quantum processor, *Nature communications* **5**, 4213 (2014).
 - [8] E. Farhi, J. Goldstone, and S. Gutmann, A quantum approximate optimization algorithm, *arXiv preprint arXiv:1411.4028* (2014).
 - [9] P. W. Shor, Polynomial-time algorithms for prime factorization and discrete logarithms on a quantum computer, *SIAM review* **41**, 303 (1999).
 - [10] S. Lloyd, Quantum approximate optimization is computationally universal, *arXiv preprint arXiv:1812.11075* (2018).
 - [11] M. E. Morales, J. D. Biamonte, and Z. Zimborás, On the universality of the quantum approximate optimization algorithm, *Quantum Information Processing* **19**, 1 (2020).
 - [12] E. Farhi and A. W. Harrow, Quantum supremacy through the quantum approximate optimization algorithm, *arXiv preprint arXiv:1602.07674* (2016).
 - [13] A. M. Dalzell, A. W. Harrow, D. E. Koh, and R. L. La Placa, How many qubits are needed for quantum computational supremacy?, *Quantum* **4**, 264 (2020).
 - [14] A. Bäertschi and S. Eidenbenz, Grover mixers for QAOA: Shifting complexity from mixer design to state preparation, in *2020 IEEE International Conference on Quantum Computing and Engineering (QCE)* (IEEE, 2020) pp. 72–82.
 - [15] S. Hadfield, Z. Wang, B. O’Gorman, E. G. Rieffel, D. Venturelli, and R. Biswas, From the quantum approximate optimization algorithm to a quantum alternating operator ansatz, *Algorithms* **12** (2019).
 - [16] J. Wurtz and P. J. Love, Classically optimal variational quantum algorithms, *IEEE Transactions on Quantum Engineering* **2**, 1 (2021).
 - [17] Z. Wang, N. C. Rubin, J. M. Dominy, and E. G. Rieffel, XY mixers: Analytical and numerical results for the quantum alternating operator ansatz, *Phys. Rev. A* **101**, 012320 (2020).
 - [18] D. J. Egger, J. Mareček, and S. Woerner, Warm-starting quantum optimization, *Quantum* **5**, 479 (2021).
 - [19] R. Tate, M. Farhadi, C. Herold, G. Mohler, and S. Gupta, Bridging classical and quantum with SDP initialized warm-starts for QAOA, *ACM Transactions on Quantum Computing* **4**, 1 (2023).
 - [20] J. Golden, A. Bäertschi, D. O’Malley, and S. Eidenbenz, Threshold-based quantum optimization, in *2021 IEEE International Conference on Quantum Computing and Engineering (QCE)* (IEEE, 2021) pp. 137–147.
 - [21] S. H. Sack and M. Serbyn, Quantum annealing initialization of the quantum approximate optimization algorithm, *Quantum* **5**, 491 (2021).
 - [22] P. Chandarana, N. N. Hegade, K. Paul, F. Albarrán-Arriagada, E. Solano, A. del Campo, and X. Chen, Digitized-counterdiabatic quantum approximate optimization algorithm, *Phys. Rev. Research* **4**, 013141 (2022).
 - [23] M. Chalupnik, H. Melo, Y. Alexeev, and A. Galda, Augmenting QAOA ansatz with multiparameter problem-independent layer, in *2022 IEEE International Conference on Quantum Computing and Engineering (QCE)* (2022) pp. 97–103.
 - [24] J. Golden, A. Bäertschi, D. O’Malley, and S. Eidenbenz, The quantum alternating operator ansatz for satisfiability problems, in *2023 IEEE International Conference on*

- Quantum Computing and Engineering (QCE)*, Vol. 01 (2023) pp. 307–312.
- [25] X. Lee, N. Xie, D. Cai, Y. Saito, and N. Asai, A depth-progressive initialization strategy for quantum approximate optimization algorithm, *Mathematics* **11**, 2176 (2023).
 - [26] S. Leontica and D. Amaro, Exploring the neighborhood of 1-layer QAOA with instantaneous quantum polynomial circuits, *Phys. Rev. Res.* **6**, 013071 (2024).
 - [27] P. K. Barkoutsos, G. Nannicini, A. Robert, I. Tavernelli, and S. Woerner, Improving Variational Quantum Optimization using CVaR, *Quantum* **4**, 256 (2020).
 - [28] L. Li, M. Fan, M. Coram, P. Riley, and S. Leichenauer, Quantum optimization with a novel Gibbs objective function and ansatz architecture search, *Phys. Rev. Res.* **2**, 023074 (2020).
 - [29] R. Majumdar, D. Madan, D. Bhoomik, D. Vinayagamurthy, S. Raghunathan, and S. Sur-Kolay, Optimizing ansatz design in QAOA for Max-cut, *arXiv preprint arXiv:2106.02812* (2021).
 - [30] R. Majumdar, D. Bhoomik, D. Madan, D. Vinayagamurthy, S. Raghunathan, and S. Sur-Kolay, Depth optimized ansatz circuit in QAOA for Max-Cut, *arXiv preprint arXiv:2110.04637* (2021).
 - [31] M. Bechtold, J. Barzen, F. Leymann, A. Mandl, J. Obst, F. Truger, and B. Weder, Investigating the effect of circuit cutting in QAOA for the MaxCut problem on NISQ devices, *Quantum Science and Technology* **8**, 045022 (2023).
 - [32] T. Peng, A. W. Harrow, M. Ozols, and X. Wu, Simulating large quantum circuits on a small quantum computer, *Phys. Rev. Lett.* **125**, 150504 (2020).
 - [33] R. Herrman, L. Treffert, J. Ostrowski, P. C. Lotshaw, T. S. Humble, and G. Siopsis, Impact of graph structures for QAOA on MaxCut, *Quantum Information Processing* **20**, 1 (2021).
 - [34] R. Shaydulin, S. Hadfield, T. Hogg, and I. Safro, Classical symmetries and the quantum approximate optimization algorithm, *Quantum Information Processing* **20**, 359 (2021).
 - [35] N. Jain, B. Coyle, E. Kashefi, and N. Kumar, Graph neural network initialisation of quantum approximate optimisation, *Quantum* **6**, 861 (2022).
 - [36] M. Streif and M. Leib, Training the quantum approximate optimization algorithm without access to a quantum processing unit, *Quantum Science and Technology* **5**, 034008 (2020).
 - [37] V. Akshay, D. Rabinovich, E. Campos, and J. Biamonte, Parameter concentrations in quantum approximate optimization, *Phys. Rev. A* **104**, L010401 (2021).
 - [38] J. Wurtz and P. J. Love, Counterdiabaticity and the quantum approximate optimization algorithm, *Quantum* **6**, 635 (2022).
 - [39] S. Bravyi, A. Kliesch, R. Koenig, and E. Tang, Obstacles to variational quantum optimization from symmetry protection, *Phys. Rev. Lett.* **125**, 260505 (2020).
 - [40] S. Bravyi, A. Kliesch, R. Koenig, and E. Tang, Hybrid quantum-classical algorithms for approximate graph coloring, *Quantum* **6**, 678 (2022).
 - [41] G. G. Guerreschi and A. Y. Matsuura, QAOA for max-cut requires hundreds of qubits for quantum speed-up, *Scientific reports* **9**, 6903 (2019).
 - [42] R. Herrman, J. Ostrowski, T. S. Humble, and G. Siopsis, Lower bounds on circuit depth of the quantum approximate optimization algorithm, *Quantum Information Processing* **20**, 59 (2021).
 - [43] J. Wurtz and D. Lykov, Fixed-angle conjectures for the quantum approximate optimization algorithm on regular maxcut graphs, *Phys. Rev. A* **104**, 052419 (2021).
 - [44] V. Akshay, H. Philathong, M. E. S. Morales, and J. D. Biamonte, Reachability deficits in quantum approximate optimization, *Phys. Rev. Lett.* **124**, 090504 (2020).
 - [45] J. Wurtz and P. Love, MaxCut quantum approximate optimization algorithm performance guarantees for $p > 1$, *Phys. Rev. A* **103**, 042612 (2021).
 - [46] E. Farhi, D. Gamarnik, and S. Gutmann, The quantum approximate optimization algorithm needs to see the whole graph: Worst case examples, *arXiv preprint arXiv:2005.08747* (2020).
 - [47] C. Xue, Z.-Y. Chen, Y.-C. Wu, and G.-P. Guo, Effects of quantum noise on quantum approximate optimization algorithm, *Chinese Physics Letters* **38**, 030302 (2021).
 - [48] S. Wang, E. Fontana, M. Cerezo, K. Sharma, A. Sone, L. Cincio, and P. J. Coles, Noise-induced barren plateaus in variational quantum algorithms, *Nature communications* **12**, 1 (2021).
 - [49] J. Marshall, F. Wudarski, S. Hadfield, and T. Hogg, Characterizing local noise in QAOA circuits, *IOP SciNotes* **1**, 025208 (2020).
 - [50] M. Alam, A. Ash-Saki, and S. Ghosh, Analysis of quantum approximate optimization algorithm under realistic noise in superconducting qubits, *arXiv preprint arXiv:1907.09631* (2019).
 - [51] M. Alam, A. Ash-Saki, and S. Ghosh, Design-space exploration of quantum approximate optimization algorithm under noise, in *2020 IEEE Custom Integrated Circuits Conference (CICC)* (IEEE, 2020) pp. 1–4.
 - [52] M. Streif, M. Leib, F. Wudarski, E. Rieffel, and Z. Wang, Quantum algorithms with local particle-number conservation: Noise effects and error correction, *Phys. Rev. A* **103**, 042412 (2021).
 - [53] E. R. Anschuetz and B. T. Kiani, Quantum variational algorithms are swamped with traps, *Nature Communications* **13**, 7760 (2022).
 - [54] D. Stilck França and R. Garcia-Patron, Limitations of optimization algorithms on noisy quantum devices, *Nature Physics* **17**, 1221 (2021).
 - [55] A. Weidinger, G. B. Mbeng, and W. Lechner, Error mitigation for quantum approximate optimization, *Phys. Rev. A* **108**, 032408 (2023).
 - [56] R. Shaydulin and A. Galda, Error mitigation for deep quantum optimization circuits by leveraging problem symmetries, in *2021 IEEE International Conference on Quantum Computing and Engineering (QCE)* (2021) pp. 291–300.
 - [57] R. Herrman, P. C. Lotshaw, J. Ostrowski, T. S. Humble, and G. Siopsis, Multi-angle quantum approximate optimization algorithm, *Scientific Reports* **12**, 6781 (2022).
 - [58] L. C. G. Govia, C. Poole, M. Saffman, and H. K. Krovi, Freedom of the mixer rotation axis improves performance in the quantum approximate optimization algorithm, *Phys. Rev. A* **104**, 062428 (2021).
 - [59] Y. Yu, C. Cao, C. Dewey, X.-B. Wang, N. Shannon, and R. Joynt, Quantum approximate optimization algorithm with adaptive bias fields, *Phys. Rev. Research* **4**, 023249 (2022).
 - [60] L. Zhu, H. L. Tang, G. S. Barron, F. A. Calderon-Vargas, N. J. Mayhall, E. Barnes, and S. E. Economou,

- Adaptive quantum approximate optimization algorithm for solving combinatorial problems on a quantum computer, *Phys. Rev. Research* **4**, 033029 (2022).
- [61] R. Tate, J. Moondra, B. Gard, G. Mohler, and S. Gupta, Warm-Started QAOA with Custom Mixers Provably Converges and Computationally Beats Goemans-Williamson’s Max-Cut at Low Circuit Depths, *Quantum* **7**, 1121 (2023).
- [62] V. Akshay, H. Philathong, I. Zacharov, and J. Biamonte, Reachability Deficits in Quantum Approximate Optimization of Graph Problems, *Quantum* **5**, 532 (2021).
- [63] M. X. Goemans and D. P. Williamson, Improved approximation algorithms for maximum cut and satisfiability problems using semidefinite programming, *Journal of the ACM (JACM)* **42**, 1115 (1995).
- [64] V. V. Vazirani, *Approximation algorithms*, Vol. 1 (Springer, 2001).
- [65] F. Barahona, M. Grötschel, M. Jünger, and G. Reinelt, An application of combinatorial optimization to statistical physics and circuit layout design, *Operations Research* **36**, 493 (1988).
- [66] R. Agrawal, S. Rajagopalan, R. Srikant, and Y. Xu, Mining newsgroups using networks arising from social behavior, in *Proceedings of the 12th International Conference on World Wide Web*, WWW ’03 (Association for Computing Machinery, New York, NY, USA, 2003) p. 529–535.
- [67] J. Poland and T. Zeugmann, Clustering pairwise distances with missing data: Maximum cuts versus normalized cuts, in *Discovery Science*, edited by L. Todarovski, N. Lavrač, and K. P. Jantke (Springer Berlin Heidelberg, Berlin, Heidelberg, 2006) pp. 197–208.
- [68] J. Wang, T. Jebara, and S.-F. Chang, Semi-supervised learning using greedy Max-Cut, *The Journal of Machine Learning Research* **14**, 771 (2013).
- [69] M. Deza and M. Laurent, Applications of cut polyhedra — i, *Journal of Computational and Applied Mathematics* **55**, 191 (1994).
- [70] M. Deza and M. Laurent, Applications of cut polyhedra — ii, *Journal of Computational and Applied Mathematics* **55**, 217 (1994).
- [71] R. M. Karp, Reducibility among combinatorial problems, in *Complexity of computer computations* (Springer, 1972) pp. 85–103.
- [72] E. Halperin, D. Livnat, and U. Zwick, MAX CUT in cubic graphs, *Journal of Algorithms* **53**, 169 (2004).
- [73] U. Feige, M. Karpinski, and M. Langberg, Improved approximation of Max-Cut on graphs of bounded degree, *Journal of Algorithms* **43**, 201 (2002).
- [74] S. Khot, On the power of unique 2-prover 1-round games, in *Proceedings of the Thirty-Fourth Annual ACM Symposium on Theory of Computing*, STOC ’02 (Association for Computing Machinery, New York, NY, USA, 2002) p. 767–775.
- [75] S. Khot, G. Kindler, E. Mossel, and R. O’Donnell, Optimal inapproximability results for MAX-CUT and other 2-variable CSPs?, *SIAM Journal on Computing* **37**, 319 (2007).
- [76] S. Khot, On the unique games conjecture (invited survey), in *2010 IEEE 25th Annual Conference on Computational Complexity* (2010) pp. 99–121.
- [77] S. A. Khot and N. K. Vishnoi, The unique games conjecture, integrality gap for cut problems and embeddability of negative-type metrics into l_1 , *Journal of the ACM (JACM)* **62**, 1 (2015).
- [78] J. Håstad, Some optimal inapproximability results, *Journal of the ACM (JACM)* **48**, 798 (2001).
- [79] L. Trevisan, G. B. Sorkin, M. Sudan, and D. P. Williamson, Gadgets, approximation, and linear programming, *SIAM Journal on Computing* **29**, 2074 (2000).
- [80] Z. Wang, S. Hadfield, Z. Jiang, and E. G. Rieffel, Quantum approximate optimization algorithm for MaxCut: A fermionic view, *Phys. Rev. A* **97**, 022304 (2018).
- [81] S. A. Hadfield, *Quantum algorithms for scientific computing and approximate optimization*, Ph.D. thesis, Columbia University (2018).
- [82] S. Hadfield, T. Hogg, and E. G. Rieffel, Analytical framework for quantum alternating operator ansätze, *Quantum Science and Technology* **8**, 015017 (2022).
- [83] A. Ozaeta, W. van Dam, and P. L. McMahon, Expectation values from the single-layer quantum approximate optimization algorithm on Ising problems, *Quantum Science and Technology* **7**, 045036 (2022).
- [84] E. Farhi, J. Goldstone, S. Gutmann, and H. Neven, Quantum algorithms for fixed qubit architectures, *arXiv preprint arXiv:1703.06199* (2017).
- [85] A. Steger and N. C. Wormald, Generating random regular graphs quickly, *Combinatorics, Probability and Computing* **8**, 377 (1999).
- [86] Gurobi Optimization, LLC, *Gurobi Optimizer Reference Manual* (2022).
- [87] Qiskit contributors, *Qiskit: An open-source framework for quantum computing* (2023).
- [88] J. Larkin, M. Jonsson, D. Justice, and G. G. Guerreschi, Evaluation of QAOA based on the approximation ratio of individual samples, *Quantum Science and Technology* **7**, 045014 (2022).
- [89] J. R. McClean, S. Boixo, V. N. Smelyanskiy, R. Babush, and H. Neven, Barren plateaus in quantum neural network training landscapes, *Nature communications* **9**, 4812 (2018).
- [90] M. J. Powell, An efficient method for finding the minimum of a function of several variables without calculating derivatives, *The computer journal* **7**, 155 (1964).
- [91] I. Gaidai and R. Herrman, Performance analysis of multi-angle QAOA for $p > 1$, *arXiv preprint arXiv:2312.00200* (2023).
- [92] Z. Holmes, K. Sharma, M. Cerezo, and P. J. Coles, Connecting ansatz expressibility to gradient magnitudes and barren plateaus, *PRX Quantum* **3**, 010313 (2022).
- [93] M. Larocca, P. Czarnik, K. Sharma, G. Muraleedharan, P. J. Coles, and M. Cerezo, Diagnosing Barren Plateaus with Tools from Quantum Optimal Control, *Quantum* **6**, 824 (2022).
- [94] Z. Allen-Zhu, Y. Li, and Z. Song, A convergence theory for deep learning via over-parameterization, in *International conference on machine learning* (PMLR, 2019) pp. 242–252.
- [95] S. Du, J. Lee, H. Li, L. Wang, and X. Zhai, Gradient descent finds global minima of deep neural networks, in *International conference on machine learning* (PMLR, 2019) pp. 1675–1685.
- [96] R.-D. Buhai, Y. Halpern, Y. Kim, A. Risteski, and D. Sontag, Empirical study of the benefits of overparameterization in learning latent variable models, in *International Conference on Machine Learning* (PMLR,

- 2020) pp. 1211–1219.
- [97] S. S. Du, X. Zhai, B. Poczos, and A. Singh, Gradient descent provably optimizes over-parameterized neural networks, [arXiv preprint arXiv:1810.02054](#) (2018).
 - [98] A. Brutzkus, A. Globerson, E. Malach, and S. Shalev-Shwartz, SGD learns over-parameterized networks that provably generalize on linearly separable data, [arXiv preprint arXiv:1710.10174](#) (2017).
 - [99] M. Larocca, N. Ju, D. García-Martín, P. J. Coles, and M. Cerezo, Theory of overparametrization in quantum neural networks, *Nature Computational Science* **3**, 542 (2023).
 - [100] A. Arrasmith, Z. Holmes, M. Cerezo, and P. J. Coles, Equivalence of quantum barren plateaus to cost concentration and narrow gorges, *Quantum Science and Technology* **7**, 045015 (2022).
 - [101] X. You, S. Chakrabarti, and X. Wu, A convergence theory for over-parameterized variational quantum eigensolvers, [arXiv preprint arXiv:2205.12481](#) (2022).
 - [102] J. Liu, K. Najafi, K. Sharma, F. Tacchino, L. Jiang, and A. Mezzacapo, Analytic theory for the dynamics of wide quantum neural networks, *Phys. Rev. Lett.* **130**, 150601 (2023).
 - [103] M. Stechly, L. Gao, B. Yogendran, E. Fontana, and M. Rudolph, Connecting the Hamiltonian structure to the QAOA energy and Fourier landscape structure, [arXiv preprint arXiv:2305.13594](#) (2023).
 - [104] B. T. Kiani, S. Lloyd, and R. Maity, Learning unitaries by gradient descent, [arXiv preprint arXiv:2001.11897](#) (2020).
 - [105] D. García-Martín, M. Larocca, and M. Cerezo, Effects of noise on the overparametrization of quantum neural networks, [arXiv preprint arXiv:2302.05059](#) (2023).
 - [106] F. G. Brandao, M. Broughton, E. Farhi, S. Gutmann, and H. Neven, For fixed control parameters the quantum approximate optimization algorithm’s objective function value concentrates for typical instances, [arXiv preprint arXiv:1812.04170](#) (2018).
 - [107] S. Sim, P. D. Johnson, and A. Aspuru-Guzik, Expressibility and entangling capability of parameterized quantum circuits for hybrid quantum-classical algorithms, *Advanced Quantum Technologies* **2**, 1900070 (2019).
 - [108] T. Haug, K. Bharti, and M. Kim, Capacity and quantum geometry of parametrized quantum circuits, *PRX Quantum* **2**, 040309 (2021).
 - [109] L. Bittel and M. Kliesch, Training variational quantum algorithms is NP-hard, *Phys. Rev. Lett.* **127**, 120502 (2021).
 - [110] L. Bittel, S. Gharibian, and M. Kliesch, The Optimal Depth of Variational Quantum Algorithms Is QCMA-Hard to Approximate, in *38th Computational Complexity Conference (CCC 2023)*, Leibniz International Proceedings in Informatics (LIPIcs), Vol. 264, edited by A. Ta-Shma (Schloss Dagstuhl – Leibniz-Zentrum für Informatik, Dagstuhl, Germany, 2023) pp. 34:1–34:24.
 - [111] S.-S. Wang, H.-L. Liu, Y.-Q. Song, F. Gao, S.-J. Qin, and Q.-Y. Wen, Quantum alternating operator ansatz for solving the minimum exact cover problem, *Physica A: Statistical Mechanics and its Applications* **626**, 129089 (2023).
 - [112] A. Bengtsson, P. Vikstål, C. Warren, M. Svensson, X. Gu, A. F. Kockum, P. Krantz, C. Križan, D. Shiri, I.-M. Svensson, G. Tancredi, G. Johansson, P. Delsing, G. Ferrini, and J. Bylander, Improved success probability with greater circuit depth for the quantum approximate optimization algorithm, *Phys. Rev. Appl.* **14**, 034010 (2020).
 - [113] J. Basso, D. Gamarnik, S. Mei, and L. Zhou, Performance and limitations of the QAOA at constant levels on large sparse hypergraphs and spin glass models, in *2022 IEEE 63rd Annual Symposium on Foundations of Computer Science (FOCS)* (IEEE Computer Society, 2022) pp. 335–343.
 - [114] S. Brandhofer, D. Braun, V. Dehn, G. Hellstern, M. Hüls, Y. Ji, I. Polian, A. S. Bhatia, and T. Wellens, Benchmarking the performance of portfolio optimization with QAOA, *Quantum Information Processing* **22**, 1 (2023).
 - [115] V. Kremenetski, T. Hogg, S. Hadfield, S. J. Cotton, and N. M. Tubman, Quantum alternating operator ansatz (QAOA) phase diagrams and applications for quantum chemistry, [arXiv preprint arXiv:2108.13056](#) (2021).
 - [116] H. Mustafa, S. N. Morapakula, P. Jain, and S. Ganguly, Variational quantum algorithms for chemical simulation and drug discovery, in *2022 International Conference on Trends in Quantum Computing and Emerging Business Technologies (TQCEBT)* (IEEE, 2022) pp. 1–8.
 - [117] K. Mesman, Z. Al-Ars, and M. Möller, Qpack: Quantum approximate optimization algorithms as universal benchmark for quantum computers, [arXiv preprint arXiv:2103.17193](#) (2021).
 - [118] L. Zhou, S.-T. Wang, S. Choi, H. Pichler, and M. D. Lukin, Quantum approximate optimization algorithm: Performance, mechanism, and implementation on near-term devices, *Phys. Rev. X* **10**, 021067 (2020).
 - [119] T. Lubinski, C. Coffrin, C. McGeoch, P. Sathe, J. Apanavicius, and D. E. B. Neira, Optimization applications as quantum performance benchmarks, [arXiv preprint arXiv:2302.02278](#) (2023).
 - [120] V. Vijendran, *XQAOA-Dataset* (2023).
 - [121] D. C. Liu and J. Nocedal, On the limited memory BFGS method for large scale optimization, *Mathematical programming* **45**, 503 (1989).
 - [122] F. Gerber and R. Furrer, optimParallel: an R package providing parallel versions of the gradient-based optimization methods of optim(), [arXiv preprint arXiv:1804.11058](#) (2018).
 - [123] M. T. Keller and W. T. Trotter, *Applied Combinatorics* (Mitchel T. Keller, William T. Trotter, 2017).

Appendix A: Goemans-Williamson (GW) Algorithm

The Goemans-Williamson algorithm [63] is a polynomial-time approximation algorithm for approximately solving the MaxCut problem. The algorithm works by constructing a semidefinite programming relaxation of the MaxCut problem and then rounding the solution to get a near-optimal cut in the original graph.

Recall in section II A that the MaxCut problem can be formulated as a binary quadratic program of the form

$$\begin{aligned}
 &\text{Maximise} && \sum_{1 \leq i < j \leq n} \frac{1}{2} w_{ij} (1 - y_i y_j) \\
 &\text{s.t} && y_i \in \{-1, 1\} \quad \forall i \in V.
 \end{aligned} \tag{A1}$$

We can relax this program to a vector program by allowing the binary variables y_i to be n -dimensional vector variables \mathbf{v}_i that lie on the n -dimensional unit sphere S_n . Replacing the product of scalar terms in eq. (A1) with the corresponding inner product, we obtain the following vector program for MaxCut.

$$\begin{aligned} & \text{Maximise} \quad \sum_{1 \leq i < j \leq n} \frac{1}{2} w_{ij} (1 - \mathbf{v}_i \cdot \mathbf{v}_j) \\ & \text{s.t} \quad \mathbf{v}_i \in S_n \quad \forall i \in V. \end{aligned} \quad (\text{A2})$$

This relaxed vector program can be efficiently solved by semidefinite programming, which allows us to obtain a set of optimal vectors \mathbf{v}_i^* for each node in the original graph. The Goeman-Williamson algorithm then uses a random n -dimensional vector \mathbf{r} from S_n to partition the vertices into two sets by assigning $\text{sign}(\mathbf{r} \cdot \mathbf{v}_i^*)$ to each node. The sign function returns 1 for non-negative inputs and -1 elsewhere, meaning that each node's rounding depends on its position relative to the hyperplane defined by \mathbf{r} that passes through the origin. The probability of the hyperplane rounding cutting an edge $\{i, j\}$ is proportional to the angle between the vectors and can be expressed as

$$\Pr[\text{sign}(\mathbf{r} \cdot \mathbf{v}_i) \neq \text{sign}(\mathbf{r} \cdot \mathbf{v}_j)] = \frac{\arccos(\mathbf{v}_i \cdot \mathbf{v}_j)}{\pi}. \quad (\text{A3})$$

The expected weight of the cut found by the algorithm is calculated by adding up the expected contributions of each edge, where the contribution of an individual edge is its probability of being cut. We can write the sum as follows

$$\begin{aligned} \mathbb{E}[W] &= \sum_{1 \leq i < j \leq n} w_{ij} \Pr[\text{sign}(\mathbf{r} \cdot \mathbf{v}_i) \neq \text{sign}(\mathbf{r} \cdot \mathbf{v}_j)] \\ &= \frac{1}{\pi} \sum_{1 \leq i < j \leq n} w_{ij} \arccos(\mathbf{v}_i \cdot \mathbf{v}_j). \end{aligned} \quad (\text{A4})$$

To find the approximation ratio, we need to compare the expected weight of the cut produced by the algorithm to the optimal cut. This is done by comparing the ratio α of individual edge contributions for each edge $\{i, j\}$ in eq. (A4) and eq. (A2) and finding the minimum value:

$$\begin{aligned} \alpha &= \frac{\arccos(\mathbf{v}_i \cdot \mathbf{v}_j)}{\pi} \frac{2}{1 - \mathbf{v}_i \cdot \mathbf{v}_j} \\ &= \frac{\theta}{\pi} \frac{2}{1 - \cos \theta}, \end{aligned} \quad (\text{A5})$$

where $\theta = \arccos(\mathbf{v}_i \cdot \mathbf{v}_j)$ is the angle between the vectors \mathbf{v}_i and \mathbf{v}_j . Minimising the above expression, we get

$$\alpha = \min_{0 \leq \theta \leq \pi} \frac{2}{\pi} \frac{\theta}{1 - \cos \theta} \approx 0.87856. \quad (\text{A6})$$

Having determined that each edge's contribution to the cut is expected to be no less than 0.87856 of the optimal

value for $\theta = 2.331122$, we can use the linearity of expectation to conclude that the total expected value is also no less than 0.87856 of the optimal value. If the Unique Games Conjecture [74–77] proves true, this method offers the strongest possible guarantee that any classical algorithm can achieve in polynomial time.

Appendix B: Parallel-LBFGS Algorithm

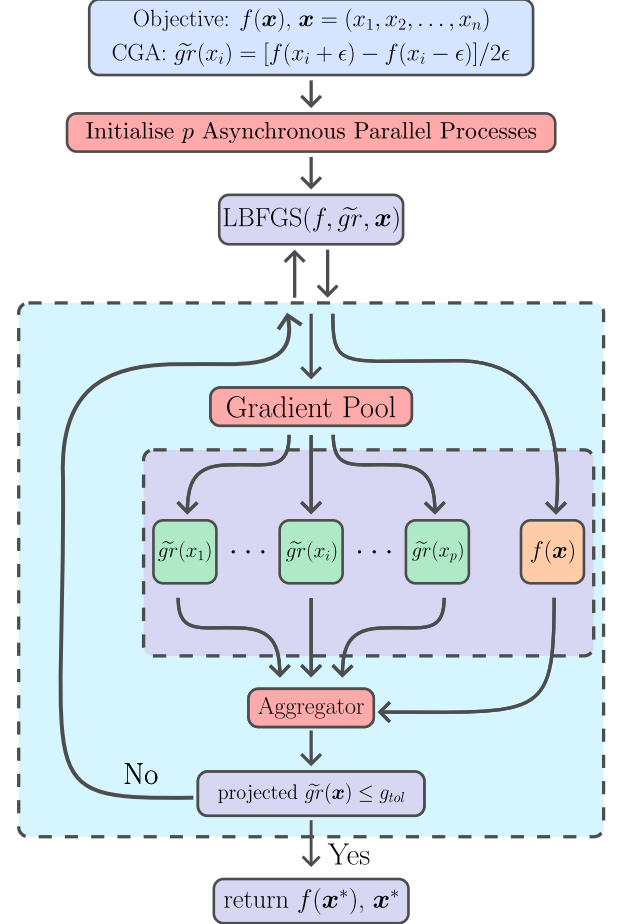


FIG. 8: The Parallel-LBFGS algorithm and CGA method are used to optimise an objective function. The objective function $f(\mathbf{x})$, gradient function $\tilde{g}r(x_i)$, and initial points $\mathbf{x} = (x_1, x_2, \dots, x_n)$ are provided to the LBFGS algorithm, which is initialised with p asynchronous processes. A gradient pool distributes the gradient calculation across p available processors. When the LBFGS algorithm calls either the objective or gradient function, the wrapper interface (blue box) begins evaluating the objective function and all the gradients in parallel. The results are then combined and returned to the LBFGS algorithm. This process is repeated until the optimisation converges to a solution (i.e., when all the gradients are less than or equal to the specified gradient tolerance value).

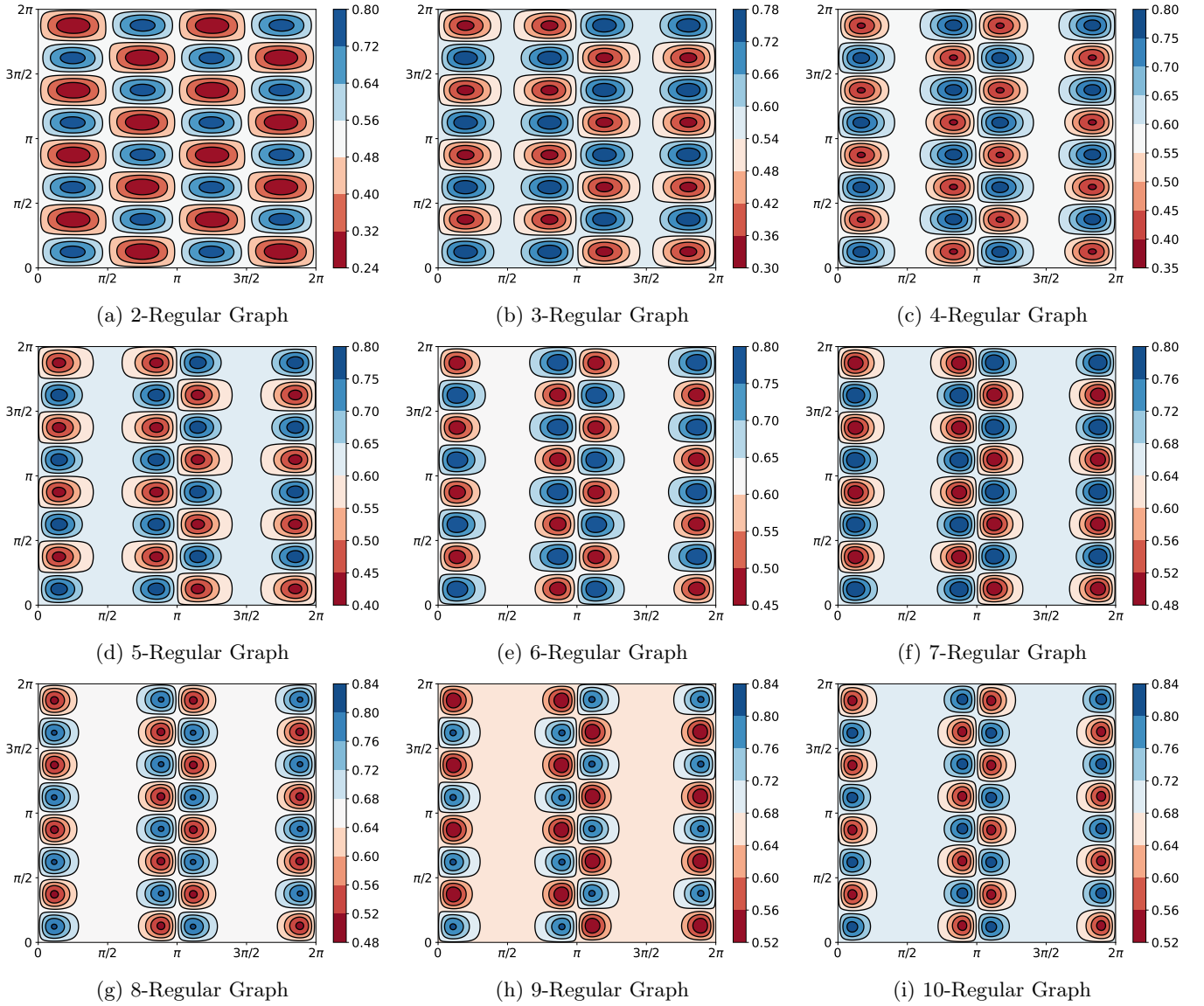


FIG. 9: The cost function for QAOA₁ ansatz for D -regular graphs with 128 vertices is plotted on contour plots for $2 \leq D \leq 10$, with the β and γ angles represented on the x and y -axis, respectively. The dark blue (red) regions represent points that maximise (minimise) the objective function. As the degree of the graph increases, the size of the barren plateaus in the cost function also increases. The barren plateaus are those lightly coloured regions without any contour lines. Despite this increase, the locations of the maxima and minima remain almost at similar locations for $0 \leq \beta \leq \frac{\pi}{4}$ and $\frac{7\pi}{4} \leq \beta \leq 2\pi$, alternating between degrees at $\frac{3\pi}{4} \leq \beta \leq \frac{5\pi}{4}$.

The XQAOA₁ and MA-QAOA₁ methods require more classical effort to identify angles that maximise the approximation ratio due to the presence of more variables to optimise. To compute the angles for QAOA₁, MA-QAOA₁, and XQAOA₁ on the collection of graphs, we used a parallel implementation of the Limited-Memory Broyden-Fletcher-Goldfarb-Shanno (LBFGS) [121] algorithm. This implementation, similar to that described in [122], utilises parallelism to compute each variable's approximate gradients and function in parallel through the use of a wrapper class that interfaces with the standard

LBFGS code. Approximate gradients are calculated using a numeric central difference gradient approximation (CGA), which requires $2n$ evaluations of the objective function if the function has n parameters. The LBFGS algorithm sequentially evaluates the objective function $1 + 2n$ times per iteration. When run on p available processor cores, the Parallel-LBFGS algorithm can evaluate all objective function calls in parallel, reducing the running time by a factor of p . Figure 8 illustrates the operation of the Parallel-LBFGS algorithm.

Appendix C: Barren-Plateau Free Classical Optimisation of QAOA Ansatz

It has been previously demonstrated in [106] that when the problem instance comes from a reasonable distribution, the cost landscape and the optimal parameters of the QAOA₁ ansatz are independent of the specific instance. This means that, for typical instances, the value of the objective function and optimal parameters are nearly the same. As a result, a strategy for finding good parameters is to take one instance of the problem and invest time and resources into finding good parameters. Although this may be computationally expensive, once this has been done, these same parameter values will result in good cost function values on other randomly chosen instances. In other words, the overall cost of solving multiple instances becomes smaller as the number of instances increases. In the case of the MaxCut problem on D -regular graphs, all graphs have this property: all vertices are connected to D other vertices. This same reasoning will apply to other combinatorial search problems that have a restriction where the number of clauses in which any variable can appear does not grow with n or at least grows only slowly with high probability.

While we are not focused on reducing the computa-

tion cost of optimising the QAOA₁ ansatz for a group of graphs, we are interested in identifying the location of the barren plateaus in the cost landscape in order to avoid choosing initial points in these areas. Figure 9 shows the contour plots of the optimisation landscape of the QAOA₁ ansatz for regular graphs with 128 vertices and degrees ranging from 2 to 10. The flat lightly coloured regions without contour lines are the barren plateaus, and it is important to avoid these areas as initial points for the classical optimiser, as failing to do so may result in the optimiser converging to a suboptimal solution and not providing the maximal solution possible using the QAOA₁ ansatz. Choosing good initial points is especially important for regular graphs with larger degrees, as the barren plateau's size increases with the graph's degree.

In the contour plots shown in fig. 9, the locations of the maxima and minima remain nearly the same for $0 \leq \beta \leq \frac{\pi}{4}$ and $\frac{7\pi}{4} \leq \beta \leq 2\pi$, alternating between degrees at $\frac{3\pi}{4} \leq \beta \leq \frac{5\pi}{4}$. Therefore, to help the classical optimiser converge on the best possible solution, we can set the initial points $\gamma \in [0, \frac{\pi}{4}]$ and $\beta \in [0, \frac{\pi}{4}]$, which will allow the classical optimiser to always converge on the optimal solution in the lower left corner of the optimisation landscape.

Appendix D: Quantifying the Performance of XQAOA, MA-QAOA, and QAOA

The goal of this appendix is to derive the analytical expressions given by eq. (22), eq. (18), and eq. (13) for the components of the XQAOA₁^{XY}, MA-QAOA and QAOA cost functions, respectively.

1. Some Useful Identities

Before proceeding with derivations of the analytical formulas, let us first state and prove some identities that will be used in this paper. We denote the set of positive integers by $\mathbb{Z}^+ = \{1, 2, \dots\}$ and the set of n -bit strings by $\mathbb{F}_2^n = \{0, 1\}^n$. When $n = 1$, we write $\mathbb{F}_2 = \mathbb{F}_2^1 = \{0, 1\}$.

Lemma 6. *Let $f \in \mathbb{Z}^+$ and $x_1, x_2, \dots, x_f, y_1, y_2, \dots, y_f \in \mathbb{R}$ be real numbers. Then,*

$$\prod_{i=1}^f \cos(x_i - y_i) = \sum_{\mu \in \mathbb{F}_2^f} \prod_{i=1}^f \cos^{1-\mu_i} x_i \cos^{1-\mu_i} y_i \sin^{\mu_i} x_i \sin^{\mu_i} y_i, \quad (\text{D1})$$

$$\prod_{i=1}^f \cos(x_i + y_i) = \sum_{\mu \in \mathbb{F}_2^f} (-1)^{|\mu|} \prod_{i=1}^f \cos^{1-\mu_i} x_i \cos^{1-\mu_i} y_i \sin^{\mu_i} x_i \sin^{\mu_i} y_i, \quad (\text{D2})$$

where $|\mu| = \sum_{i=1}^f \mu_i$.

Proof. The first identity eq. (D1) follows from recognising that for any $a, b \in \mathbb{R}$, the sum $a + b$ can be written as the following sum of products:

$$a + b = \sum_{\mu \in \mathbb{F}_2} a^{1-\mu} b^{\mu}. \quad (\text{D3})$$

Applying eq. (D3) to each term of the sum $\cos x_i \cos y_i + \sin x_i \sin y_i$ gives

$$\begin{aligned} \prod_{i=1}^f \cos(x_i - y_i) &= \prod_{i=1}^f (\cos x_i \cos y_i + \sin x_i \sin y_i) \\ &= \prod_{i=1}^f \sum_{\mu_i \in \mathbb{F}_2} \cos^{1-\mu_i} x_i \cos^{1-\mu_i} y_i \sin^{\mu_i} x_i \sin^{\mu_i} y_i \\ &= \sum_{\mu \in \mathbb{F}_2^f} \prod_{i=1}^f \cos^{1-\mu_i} x_i \cos^{1-\mu_i} y_i \sin^{\mu_i} x_i \sin^{\mu_i} y_i. \end{aligned}$$

The identity in eq. (D2) follows immediately from replacing each y_i in eq. (D1) with $-y_i$. \square

By taking the sum (difference, respectively) of eq. (D1) and eq. (D2), only the even (odd, respectively) terms remain. Hence, it follows that

Lemma 7. *Let $f \in \mathbb{Z}^+$ and $x_1, x_2, \dots, x_f, y_1, y_2, \dots, y_f \in \mathbb{R}$. Then, we have that*

$$\prod_{i=1}^f \cos(x_i - y_i) + \prod_{i=1}^f \cos(x_i + y_i) = 2 \sum_{\substack{\mu \in \mathbb{F}_2^f \\ |\mu| \text{ even}}} \prod_{i=1}^f \cos^{1-\mu_i} x_i \cos^{1-\mu_i} y_i \sin^{\mu_i} x_i \sin^{\mu_i} y_i, \quad (\text{D4})$$

$$\prod_{i=1}^f \cos(x_i - y_i) - \prod_{i=1}^f \cos(x_i + y_i) = 2 \sum_{\substack{\mu \in \mathbb{F}_2^f \\ |\mu| \text{ odd}}} \prod_{i=1}^f \cos^{1-\mu_i} x_i \cos^{1-\mu_i} y_i \sin^{\mu_i} x_i \sin^{\mu_i} y_i. \quad (\text{D5})$$

We now make a remark about the above identities: while the right-hand sides of eq. (D1), eq. (D2), eq. (D4), and eq. (D5) each involves a sum over exponentially (in f) many terms (the cardinality of \mathbb{F}_2^f is 2^f), their left-hand sides involve just products of polynomially (in f) many terms. Hence, going from the right-hand sides of these identities to their left-hand sides results in exponential savings in computational cost. This will be useful for the expressions that we derive in appendix D2.

2. Proof of theorem 3

Proof of theorem 3. Consider the XQAOA ansatz applied to MaxCut with $|s\rangle = |+\rangle^{\otimes n}$ and $Q = e^{-i\alpha \cdot \mathbf{Y}} e^{-i\beta \cdot \mathbf{X}} e^{-i\gamma \cdot \mathbf{C}}$, where $\alpha \cdot \mathbf{Y} = \sum_{i=1}^n \alpha_i Y_i$, $\beta \cdot \mathbf{X} = \sum_{i=1}^n \beta_i X_i$, and $\gamma \cdot \mathbf{C} = \sum_{\{u,v\} \in E} \gamma_{uv} C_{uv} = \frac{1}{2} \sum_{\{u,v\} \in E} \gamma_{uv} w_{uv} (I - Z_u Z_v)$.

Observe that

$$\langle C \rangle_{XY} = \langle s | Q^\dagger C Q | s \rangle = \sum_{\{u,v\} \in E} \frac{w_{uv}}{2} - \frac{w_{uv}}{2} \langle s | Q^\dagger Z_u Z_v Q | s \rangle. \quad (\text{D6})$$

Hence, to compute the expectation value $\langle C \rangle_{XY}$, it suffices to compute each term

$$\langle C_{uv} \rangle_{XY} := \frac{w_{uv}}{2} - \frac{w_{uv}}{2} \langle s | Q^\dagger Z_u Z_v Q | s \rangle \quad (\text{D7})$$

in the sum separately.

For the rest of this proof, we fix an edge $\{u, v\} \in E$. We shall evaluate the product $Q^\dagger Z_u Z_v Q$ in eq. (D7) by conjugating the Pauli operator $Z_u Z_v$ by the mixing unitary and then by the problem unitary. By the commutation properties of the Pauli matrices Λ and the fact that they satisfy $e^{-i\theta\Lambda} = \cos\theta I - i\sin\theta\Lambda$, it follows that most of the terms in the mixing unitary $e^{-i\alpha \cdot \mathbf{Y}} e^{-i\beta \cdot \mathbf{X}} = \prod_{j=1}^n e^{-i\alpha_j Y_j} e^{-i\beta_j X_j}$ commute through $Z_u Z_v$ and annihilate their inverses. Hence,

$$e^{i\beta \cdot \mathbf{X}} e^{i\alpha \cdot \mathbf{Y}} Z_u Z_v e^{-i\alpha \cdot \mathbf{Y}} e^{-i\beta \cdot \mathbf{X}} = (e^{i\beta_u X_u} e^{2i\alpha_u Y_u} e^{i\beta_u X_u} Z_u) \otimes (e^{i\beta_v X_v} e^{2i\alpha_v Y_v} e^{i\beta_v X_v} Z_v). \quad (\text{D8})$$

The factors in the above Kronecker product can be expanded as follows. For $a \in \{u, v\}$,

$$\begin{aligned} e^{i\beta_a X_a} e^{2i\alpha_a Y_a} e^{i\beta_a X_a} Z_a &= (\cos \beta_a + i \sin \beta_a X_a) (\cos 2\alpha_a + i \sin 2\alpha_a Y_a) (\cos \beta_a + i \sin \beta_a X_a) Z_a \\ &= \cos 2\alpha_a \cos 2\beta_a Z_a + \cos 2\alpha_a \sin 2\beta_a Y_a - \sin 2\alpha_a X_a. \end{aligned} \quad (D9)$$

Substituting this into equation eq. (D8) gives

$$\begin{aligned} e^{i\beta \cdot \mathbf{X}} e^{i\alpha \cdot \mathbf{Y}} Z_u Z_v e^{-i\alpha \cdot \mathbf{Y}} e^{-i\beta \cdot \mathbf{X}} &= \cos 2\alpha_u \cos 2\beta_u \cos 2\alpha_v \cos 2\beta_v Z_u Z_v + \cos 2\alpha_u \cos 2\beta_u \cos 2\alpha_v \sin 2\beta_v Z_u Y_v \\ &\quad - \cos 2\alpha_u \cos 2\beta_u \sin 2\alpha_v Z_u X_v + \cos 2\alpha_u \sin 2\beta_u \cos 2\alpha_v \cos 2\beta_v Y_u Z_v \\ &\quad + \cos 2\alpha_u \sin 2\beta_u \cos 2\alpha_v \sin 2\beta_v Y_u Y_v - \cos 2\alpha_u \sin 2\beta_u \sin 2\alpha_v Y_u X_v \\ &\quad - \sin 2\alpha_u \cos 2\alpha_v \cos 2\beta_v X_u Z_v - \sin 2\alpha_u \cos 2\alpha_v \sin 2\beta_v X_u Y_v \\ &\quad + \sin 2\alpha_u \sin 2\alpha_v X_u X_v. \end{aligned} \quad (D10)$$

Hence, by substituting this expression into eq. (D7), the expected cost function corresponding to the edge $\{u, v\} \in E$ can be written as

$$\begin{aligned} \langle C_{uv} \rangle_{XY} &= \frac{w_{uv}}{2} - \frac{w_{uv}}{2} \left\{ \cos 2\alpha_u \cos 2\beta_u \cos 2\alpha_v \cos 2\beta_v \xi(Z, Z) + \cos 2\alpha_u \cos 2\beta_u \cos 2\alpha_v \sin 2\beta_v \xi(Z, Y) \right. \\ &\quad - \cos 2\alpha_u \cos 2\beta_u \sin 2\alpha_v \xi(Z, X) + \cos 2\alpha_u \sin 2\beta_u \cos 2\alpha_v \cos 2\beta_v \xi(Y, Z) \\ &\quad + \cos 2\alpha_u \sin 2\beta_u \cos 2\alpha_v \sin 2\beta_v \xi(Y, Y) - \cos 2\alpha_u \sin 2\beta_u \sin 2\alpha_v \xi(Y, X) \\ &\quad - \sin 2\alpha_u \cos 2\alpha_v \cos 2\beta_v \xi(X, Z) - \sin 2\alpha_u \cos 2\alpha_v \sin 2\beta_v \xi(X, Y) \\ &\quad \left. + \sin 2\alpha_u \sin 2\alpha_v \xi(X, X) \right\}, \end{aligned} \quad (D11)$$

where for single-qubit Pauli matrices $P, Q \in \{X, Y, Z\}$, we have defined

$$\xi(P, Q) = \langle s | \eta(P, Q) | s \rangle, \quad (D12)$$

$$\eta(P, Q) = e^{i\gamma \cdot \mathbf{C}} P_u Q_v e^{-i\gamma \cdot \mathbf{C}}. \quad (D13)$$

Moving forward, the approach we take is as follows. Firstly, we shall evaluate the expression for $\eta(P, Q)$ in eq. (D13) for all $P, Q \in \{X, Y, Z\}$. Secondly, we shall substitute our expressions for $\eta(P, Q)$ into eq. (D12) to derive analytical expressions for $\xi(P, Q)$. Thirdly and also finally, we shall substitute these analytical expressions into eq. (D11) to obtain our desired expression eq. (22).

Before we execute these three steps, we first introduce some notation to help us keep track of the neighbours of the edge $\{u, v\}$: let

$$\mathcal{N}_{u \setminus v} = \mathcal{N}(u) \setminus (\mathcal{N}(v) \cup \{v\}) = \{\omega_1, \omega_2, \dots, \omega_b\} \quad (D14)$$

be the set of neighbors of u that are of distance 2 or greater from v . Similarly, let

$$\mathcal{N}_{v \setminus u} = \mathcal{N}(v) \setminus (\mathcal{N}(u) \cup \{u\}) = \{q_1, q_2, \dots, q_c\} \quad (D15)$$

be the set of neighbors of v that are of distance 2 or greater from u . Next, let

$$\mathcal{N}_{uv} = \mathcal{N}(u) \cap \mathcal{N}(v) = \{a_1, a_2, \dots, a_f\} = \{\omega_{b+1}, \omega_{b+2}, \dots, \omega_d\} = \{q_{c+1}, q_{c+2}, \dots, q_e\}, \quad (D16)$$

where $a_i = \omega_{b+i} = q_{c+i}$ for $i = 1, \dots, f$, be the set of vertices that are neighbours of both u and v , i.e., \mathcal{N}_{uv} comprises those nodes in V that form a triangle with both u and v . Finally, let

$$\mathcal{N}_{u \setminus v} = \mathcal{N}(u) \setminus \{v\} = \mathcal{N}_{u \setminus v} \cup \mathcal{N}_{uv} = \{\omega_1, \dots, \omega_b, a_1, \dots, a_f\} = \{\omega_1, \dots, \omega_b, \dots, \omega_d\} \quad (D17)$$

be the set of neighbours of u that are not v and let

$$\mathcal{N}_{v \setminus u} = \mathcal{N}_{v \setminus u} \cup \mathcal{N}_{uv} = \{q_1, \dots, q_c, a_1, \dots, a_f\} = \{q_1, \dots, q_c, \dots, q_e\} \quad (D18)$$

be the set of neighbours of v that are not u . We are now ready to execute our aforementioned three steps.

Step 1: Evaluation of $\eta(P, Q)$

First, we rewrite eq. (D13) as

$$\eta(P, Q) = e^{i\gamma \cdot C'} P_u Q_v e^{-i\gamma \cdot C'}, \quad (\text{D19})$$

where

$$\gamma \cdot C' = \sum_{\{x,y\} \in E} \gamma_{xy} C'_{xy}, \quad C'_{xy} = -\frac{1}{2} w_{xy} Z_x Z_y, \quad (\text{D20})$$

since the term $\frac{1}{2} \sum_{\{u,v\} \in E} \gamma_{uv} w_{uv} I$ in C_{uv} is cancelled by its inverse and does not contribute to eq. (D13). Next, we expand $\gamma \cdot C'$ as

$$\gamma \cdot C' = \gamma_{uv} C'_{uv} + \gamma \cdot C'_u + \gamma \cdot C'_v + \sum_{\{x,y\} \in E_{(uv)}} \gamma_{xy} C'_{xy}, \quad (\text{D21})$$

where

$$\gamma \cdot C'_u = \sum_{i=1}^d \gamma_{u\omega_i} C'_{u\omega_i} = \sum_{i=1}^b \gamma_{u\omega_i} C'_{u\omega_i} + \sum_{i=1}^f \gamma_{ua_i} C'_{ua_i} \quad (\text{D22})$$

contains terms involving u but not v , and

$$\gamma \cdot C'_v = \sum_{i=1}^e \gamma_{vq_i} C'_{vq_i} = \sum_{i=1}^c \gamma_{vq_i} C'_{vq_i} + \sum_{i=1}^f \gamma_{va_i} C'_{va_i} \quad (\text{D23})$$

contains terms involving v but not u , and $E_{(uv)} = \{\{a,b\} \in E : a, b \notin \{u,v\}\}$ denotes the set of edges that do not contain either u or v as an endpoint. By substituting eq. (D21) into eq. (D19), we obtain

$$\eta(P, Q) = e^{i\gamma \cdot C'_u} e^{i\gamma \cdot C'_v} e^{i\gamma_{uv} C'_{uv}} P_u Q_v e^{-i\gamma_{uv} C'_{uv}} e^{-i\gamma \cdot C'_v} e^{-i\gamma \cdot C'_u} = \Gamma_{PQ} P_u Q_v, \quad (\text{D24})$$

where $\Gamma_{PQ} = \eta(P, Q) P_u Q_v$. By using the fact that Pauli operators either commute or anti-commute, evaluating eq. (D24) gives

$$\Gamma_{XX} = \Gamma_{XY} = \Gamma_{YX} = \Gamma_{YY} = e^{2i\gamma \cdot C'_u} e^{2i\gamma \cdot C'_v}, \quad (\text{D25})$$

$$\Gamma_{XZ} = \Gamma_{YZ} = e^{2i\gamma_{uv} C'_{uv}} e^{2i\gamma \cdot C'_u}, \quad (\text{D26})$$

$$\Gamma_{ZX} = \Gamma_{ZY} = e^{2i\gamma_{uv} C'_{uv}} e^{2i\gamma \cdot C'_v}, \quad (\text{D27})$$

$$\Gamma_{ZZ} = I. \quad (\text{D28})$$

To evaluate eq. (D25), we first compute

$$\begin{aligned} e^{2i\gamma \cdot C'_u} &= \prod_{i=1}^d [\cos(\gamma_{u\omega_i} w_{u\omega_i}) I - i \sin(\gamma_{u\omega_i} w_{u\omega_i}) Z_u Z_{\omega_i}] \\ &= \sum_{x \in \mathbb{F}_2^d} \cos^{1-x_1}(\gamma_{u\omega_1} w_{u\omega_1}) \cdots \cos^{1-x_d}(\gamma_{u\omega_d} w_{u\omega_d}) [-i \sin(\gamma_{u\omega_1} w_{u\omega_1})]^{x_1} \cdots [-i \sin(\gamma_{u\omega_d} w_{u\omega_d})]^{x_d} Z_u^{|x|} Z_{\omega_1}^{x_1} \cdots Z_{\omega_d}^{x_d}, \end{aligned} \quad (\text{D29})$$

where we applied the trick in eq. (D3) to each term in the above product. In the above expression, $|x| = \sum_{i=1}^d x_i$ denotes the Hamming weight of the string $x \in \{0, 1\}^d$. Similarly,

$$e^{2i\gamma \cdot C'_v} = \sum_{y \in \mathbb{F}_2^e} \cos^{1-y_1}(\gamma_{vq_1} w_{vq_1}) \cdots \cos^{1-y_e}(\gamma_{vq_e} w_{vq_e}) [-i \sin(\gamma_{vq_1} w_{vq_1})]^{y_1} \cdots [-i \sin(\gamma_{vq_e} w_{vq_e})]^{y_e} Z_v^{|y|} Z_{q_1}^{y_1} \cdots Z_{q_e}^{y_e}. \quad (\text{D30})$$

By taking the product of eq. (D29) and eq. (D30), and using eq. (D16) to relabel the vertices in \mathcal{N}_{uv} by a_i 's, we obtain the following expression for eq. (D25):

$$\begin{aligned} \Gamma_{XX} = & \sum_{\alpha \in \mathbb{F}_2^b} \sum_{\beta \in \mathbb{F}_2^c} \sum_{\mu \in \mathbb{F}_2^f} \sum_{\nu \in \mathbb{F}_2^f} \cos^{1-\alpha_1}(\gamma_{u\omega_1} w_{u\omega_1}) \cdots \cos^{1-\alpha_b}(\gamma_{u\omega_b} w_{u\omega_b}) \cos^{1-\mu_1}(\gamma_{ua_1} w_{ua_1}) \cdots \cos^{1-\mu_f}(\gamma_{ua_f} w_{ua_f}) \\ & \times \cos^{1-\beta_1}(\gamma_{vq_1} w_{vq_1}) \cdots \cos^{1-\beta_c}(\gamma_{vq_c} w_{vq_c}) \cos^{1-\nu_1}(\gamma_{va_1} w_{va_1}) \cdots \cos^{1-\nu_f}(\gamma_{va_f} w_{va_f}) \\ & \times [-i \sin(\gamma_{u\omega_1} w_{u\omega_1})]^{\alpha_1} \cdots [-i \sin(\gamma_{u\omega_b} w_{u\omega_b})]^{\alpha_b} [-i \sin(\gamma_{ua_1} w_{ua_1})]^{\mu_1} \cdots [-i \sin(\gamma_{ua_f} w_{ua_f})]^{\mu_f} \\ & \times [-i \sin(\gamma_{vq_1} w_{vq_1})]^{\beta_1} \cdots [-i \sin(\gamma_{vq_c} w_{vq_c})]^{\beta_c} [-i \sin(\gamma_{va_1} w_{va_1})]^{\nu_1} \cdots [-i \sin(\gamma_{va_f} w_{va_f})]^{\nu_f} \\ & \times Z_u^{|\alpha|+|\mu|} \cdot Z_v^{|\beta|+|\nu|} \cdot \prod_{i=1}^b Z_{\omega_i}^{\alpha_i} \cdot \prod_{i=1}^c Z_{q_i}^{\beta_i} \cdot \prod_{i=1}^f Z_{a_i}^{\mu_i+\nu_i}. \end{aligned} \quad (\text{D31})$$

Next, by substituting eq. (D29) into eq. (D26), we obtain

$$\begin{aligned} \Gamma_{XZ} = & \sum_{x_0 x_1 \dots x_d \in \mathbb{F}_2^{d+1}} \cos^{1-x_0}(\gamma_{uv} w_{uv}) \cos^{1-x_1}(\gamma_{u\omega_1} w_{u\omega_1}) \cdots \cos^{1-x_d}(\gamma_{u\omega_d} w_{u\omega_d}) \\ & \times [-i \sin(\gamma_{uv} w_{uv})]^{x_0} [-i \sin(\gamma_{u\omega_1} w_{u\omega_1})]^{x_1} \cdots [-i \sin(\gamma_{u\omega_d} w_{u\omega_d})]^{x_d} Z_u^{|x|} Z_v^{x_0} Z_{\omega_1}^{x_1} \cdots Z_{\omega_d}^{x_d}. \end{aligned} \quad (\text{D32})$$

Similarly, by substituting eq. (D30) into eq. (D27), we obtain

$$\begin{aligned} \Gamma_{ZX} = & \sum_{y_0 y_1 \dots y_e \in \mathbb{F}_2^{e+1}} \cos^{1-y_0}(\gamma_{uv} w_{uv}) \cos^{1-y_1}(\gamma_{vq_1} w_{vq_1}) \cdots \cos^{1-y_e}(\gamma_{vq_e} w_{vq_e}) \\ & \times [-i \sin(\gamma_{uv} w_{uv})]^{y_0} [-i \sin(\gamma_{vq_1} w_{vq_1})]^{y_1} \cdots [-i \sin(\gamma_{vq_e} w_{vq_e})]^{y_e} Z_u^{y_0} Z_v^{|y|} Z_{q_1}^{y_1} \cdots Z_{q_e}^{y_e}. \end{aligned} \quad (\text{D33})$$

This completes Step 1, where $\eta(P, Q)$ is specified by eq. (D24), eq. (D31), eq. (D32), eq. (D33), and eq. (D28).

Step 2: Evaluation of $\xi(P, Q)$

There are $3^2 = 9$ different choices of $PQ \in \{X, Y, Z\}^2$. We will split these choices into four cases, as follows:

- Case 1: $PQ = XX, XY, YX, YY$. By substituting eq. (D24) and eq. (D31) into eq. (D12), we obtain

$$\begin{aligned} \xi(P, Q) = & \sum_{\alpha \in \mathbb{F}_2^b} \sum_{\beta \in \mathbb{F}_2^c} \sum_{\mu \in \mathbb{F}_2^f} \sum_{\nu \in \mathbb{F}_2^f} \cos^{1-\alpha_1}(\gamma_{u\omega_1} w_{u\omega_1}) \cdots \cos^{1-\alpha_b}(\gamma_{u\omega_b} w_{u\omega_b}) \cos^{1-\mu_1}(\gamma_{ua_1} w_{ua_1}) \cdots \cos^{1-\mu_f}(\gamma_{ua_f} w_{ua_f}) \\ & \times \cos^{1-\beta_1}(\gamma_{vq_1} w_{vq_1}) \cdots \cos^{1-\beta_c}(\gamma_{vq_c} w_{vq_c}) \cos^{1-\nu_1}(\gamma_{va_1} w_{va_1}) \cdots \cos^{1-\nu_f}(\gamma_{va_f} w_{va_f}) \\ & \times [-i \sin(\gamma_{u\omega_1} w_{u\omega_1})]^{\alpha_1} \cdots [-i \sin(\gamma_{u\omega_b} w_{u\omega_b})]^{\alpha_b} [-i \sin(\gamma_{ua_1} w_{ua_1})]^{\mu_1} \cdots [-i \sin(\gamma_{ua_f} w_{ua_f})]^{\mu_f} \\ & \times [-i \sin(\gamma_{vq_1} w_{vq_1})]^{\beta_1} \cdots [-i \sin(\gamma_{vq_c} w_{vq_c})]^{\beta_c} [-i \sin(\gamma_{va_1} w_{va_1})]^{\nu_1} \cdots [-i \sin(\gamma_{va_f} w_{va_f})]^{\nu_f} \\ & \times \underbrace{\text{tr} \left\{ |s\rangle\langle s| Z_u^{|\alpha|+|\mu|} P_u \cdot Z_v^{|\beta|+|\nu|} Q_v \cdot \prod_{i=1}^b Z_{\omega_i}^{\alpha_i} \cdot \prod_{i=1}^c Z_{q_i}^{\beta_i} \cdot \prod_{i=1}^f Z_{a_i}^{\mu_i+\nu_i} \right\}}_{\textcircled{1}}. \end{aligned} \quad (\text{D34})$$

By writing the initial state as $|s\rangle\langle s| = \bigotimes_{j=1}^n \frac{1}{2}(I + X_j)$, the last line of eq. (D34) can be expanded as

$$\begin{aligned} \textcircled{1} = & \text{tr} \left\{ \frac{I + X_u}{2} Z_u^{|\alpha|+|\mu|} P_u \right\} \text{tr} \left\{ \frac{I + X_v}{2} Z_v^{|\beta|+|\nu|} Q_v \right\} \\ & \times \prod_{i=1}^b \underbrace{\text{tr} \left\{ \frac{I + X_{\omega_i}}{2} Z_{\omega_i}^{\alpha_i} \right\}}_{=\delta_{\alpha_i, 0}} \prod_{i=1}^c \underbrace{\text{tr} \left\{ \frac{I + X_{q_i}}{2} Z_{q_i}^{\beta_i} \right\}}_{=\delta_{\beta_i, 0}} \prod_{i=1}^f \underbrace{\text{tr} \left\{ \frac{I + X_{a_i}}{2} Z_{a_i}^{\mu_i+\nu_i} \right\}}_{=\delta_{\mu_i, \nu_i}} \\ = & \underbrace{\text{tr} \left\{ \frac{I + X_u}{2} Z_u^{|\mu|} P_u \right\}}_{\textcircled{2}} \underbrace{\text{tr} \left\{ \frac{I + X_v}{2} Z_v^{|\nu|} Q_v \right\}}_{\textcircled{3}} \prod_{i=1}^b \delta_{\alpha_i, 0} \prod_{i=1}^c \delta_{\beta_i, 0} \prod_{i=1}^f \delta_{\mu_i, \nu_i}. \end{aligned} \quad (\text{D35})$$

Now, for $P \in \{X, Y\}$ and for $|\mu| \in \mathbb{N}$,

$$\textcircled{2} = [P = X][|\mu| \text{ even}] - i[P = Y][|\mu| \text{ odd}], \quad (\text{D36})$$

where the $[A]$ denotes the Iverson bracket of statement A ; i.e. $[A] = 1$ if A is true and 0 otherwise. Similarly,

$$\textcircled{3} = [Q = X][|\mu| \text{ even}] - i[Q = Y][|\mu| \text{ odd}]. \quad (\text{D37})$$

Hence, the product of eq. (D36) and eq. (D37) is

$$\textcircled{2} \times \textcircled{3} = [P = Q = X][|\mu| \text{ even}] - [P = Q = Y][|\mu| \text{ odd}]. \quad (\text{D38})$$

Substituting eq. (D38) into eq. (D35) gives

$$\textcircled{1} = \delta_{\alpha,0} \delta_{\beta,0} \delta_{\mu,\nu} ([P = Q = X][|\mu| \text{ even}] - [P = Q = Y][|\mu| \text{ odd}]). \quad (\text{D39})$$

Substituting eq. (D39) into eq. (D34) and using the Kronecker deltas to eliminate terms in the sum, we get

$$\begin{aligned} \xi(P, Q) &= \sum_{\mu \in \mathbb{F}_2^f} \cos(\gamma_{u\omega_1} w_{u\omega_1}) \cdots \cos(\gamma_{u\omega_b} w_{u\omega_b}) \cos^{1-\mu_1}(\gamma_{ua_1} w_{ua_1}) \cdots \cos^{1-\mu_f}(\gamma_{ua_f} w_{ua_f}) \\ &\quad \times \cos(\gamma_{vq_1} w_{vq_1}) \cdots \cos(\gamma_{vq_c} w_{vq_c}) \cos^{1-\mu_1}(\gamma_{va_1} w_{va_1}) \cdots \cos^{1-\mu_f}(\gamma_{va_f} w_{va_f}) \\ &\quad \times (-i)^{2|\mu|} \sin^{\mu_1}(\gamma_{ua_1} w_{ua_1}) \cdots \sin^{\mu_f}(\gamma_{ua_f} w_{ua_f}) \sin^{\mu_1}(\gamma_{va_1} w_{va_1}) \cdots \sin^{\mu_f}(\gamma_{va_f} w_{va_f}) \\ &\quad \times ([P = Q = X][|\mu| \text{ even}] - [P = Q = Y][|\mu| \text{ odd}]) \\ &= \prod_{\omega \in \mathcal{N}_u \setminus v} \cos(\gamma_{u\omega} w_{u\omega}) \prod_{q \in \mathcal{N}_v \setminus u} \cos(\gamma_{vq} w_{vq}) \left([P = Q = X] \sum_{\substack{\mu \in \mathbb{F}_2^f \\ |\mu| \text{ even}}} + [P = Q = Y] \sum_{\substack{\mu \in \mathbb{F}_2^f \\ |\mu| \text{ odd}}} \right) \\ &\quad \prod_{i=1}^f \cos^{1-\mu_i}(\gamma_{ua_i} w_{ua_i}) \cos^{1-\mu_i}(\gamma_{va_i} w_{va_i}) \sin^{\mu_i}(\gamma_{ua_i} w_{ua_i}) \sin^{\mu_i}(\gamma_{va_i} w_{va_i}). \end{aligned} \quad (\text{D40})$$

Since the Iverson brackets in eq. (D40) vanish when $PQ = XY$ or YX , it follows that

$$\xi(X, Y) = \xi(Y, X) = 0. \quad (\text{D41})$$

When $PQ = XX$, eq. (D40) reduces to

$$\begin{aligned} \xi(X, X) &= \prod_{\omega \in \mathcal{N}_u \setminus v} \cos(\gamma_{u\omega} w_{u\omega}) \prod_{q \in \mathcal{N}_v \setminus u} \cos(\gamma_{vq} w_{vq}) \\ &\quad \times \sum_{\substack{\mu \in \mathbb{F}_2^f \\ |\mu| \text{ even}}} \prod_{i=1}^f \cos^{1-\mu_i}(\gamma_{ua_i} w_{ua_i}) \cos^{1-\mu_i}(\gamma_{va_i} w_{va_i}) \sin^{\mu_i}(\gamma_{ua_i} w_{ua_i}) \sin^{\mu_i}(\gamma_{va_i} w_{va_i}) \\ &= \frac{1}{2} \prod_{\omega \in \mathcal{N}_u \setminus v} \cos(\gamma_{u\omega} w_{u\omega}) \prod_{q \in \mathcal{N}_v \setminus u} \cos(\gamma_{vq} w_{vq}) \\ &\quad \times \left[\prod_{i=1}^f \cos(\gamma_{ua_i} w_{ua_i} + \gamma_{va_i} w_{va_i}) + \prod_{i=1}^f \cos(\gamma_{ua_i} w_{ua_i} - \gamma_{va_i} w_{va_i}) \right] \\ &= \frac{1}{2} \prod_{\omega \in \mathcal{N}_u \setminus v} \cos(\gamma_{u\omega} w_{u\omega}) \prod_{q \in \mathcal{N}_v \setminus u} \cos(\gamma_{vq} w_{vq}) \\ &\quad \times \left[\prod_{q \in \mathcal{N}_{uv}} \cos(\gamma_{uq} w_{uq} - \gamma_{vq} w_{vq}) + \prod_{q \in \mathcal{N}_{uv}} \cos(\gamma_{uq} w_{uq} + \gamma_{vq} w_{vq}) \right], \end{aligned} \quad (\text{D42})$$

where the second equality follows from eq. (D4).

Similarly, for the case $PQ = YY$, utilising eq. (D5) gives

$$\begin{aligned} \xi(Y, Y) &= \frac{1}{2} \prod_{\omega \in \mathcal{N}_u \setminus v} \cos(\gamma_{u\omega} w_{u\omega}) \prod_{q \in \mathcal{N}_v \setminus u} \cos(\gamma_{vq} w_{vq}) \\ &\quad \times \left[\prod_{q \in \mathcal{N}_{uv}} \cos(\gamma_{uq} w_{uq} - \gamma_{vq} w_{vq}) - \prod_{q \in \mathcal{N}_{uv}} \cos(\gamma_{uq} w_{uq} + \gamma_{vq} w_{vq}) \right], \end{aligned} \quad (\text{D43})$$

which differs from the expression given by eq. (D42) for $\xi(X, X)$ by only a single minus sign. As we mentioned in appendix D1, the identities eq. (D4) and eq. (D5) allowed us to simplify the exponential sums in eq. (D40) to get exponential savings in the computational cost in the worst case.

- Case 2: $PQ = XZ, YZ$. By substituting eq. (D24) and eq. (D32) into eq. (D12), we obtain, for $P = X, Y$,

$$\begin{aligned} \xi(P, Z) &= \sum_{x_0 x_1 \dots x_d \in \mathbb{F}_2^{d+1}} \cos^{1-x_0}(\gamma_{uv} w_{uv}) \cos^{1-x_1}(\gamma_{u\omega_1} w_{u\omega_1}) \dots \cos^{1-x_d}(\gamma_{u\omega_d} w_{u\omega_d}) \\ &\quad \times [-i \sin(\gamma_{uv} w_{uv})]^{x_0} [-i \sin(\gamma_{u\omega_1} w_{u\omega_1})]^{x_1} \dots [-i \sin(\gamma_{u\omega_d} w_{u\omega_d})]^{x_d} \\ &\quad \times \underbrace{\text{tr} \left\{ |s\rangle\langle s| Z_u^{x_0} P_u Z_v^{x_0+1} Z_{\omega_1}^{x_1} \dots Z_{\omega_d}^{x_d} \right\}}_{\textcircled{4}}. \end{aligned} \quad (\text{D44})$$

By writing $|s\rangle\langle s| = \bigotimes_{j=1}^n \frac{1}{2}(I + X_j)$, the last line of eq. (D44) can be expanded as

$$\begin{aligned} \textcircled{4} &= \text{tr} \left\{ \frac{I + X_u}{2} Z_u^{x_0+x_1+\dots+x_d} P_u \right\} \text{tr} \left\{ \frac{I + X_v}{2} Z_v^{x_0+1} \right\} \prod_{i=1}^d \underbrace{\text{tr} \left\{ \frac{I + X_{\omega_i}}{2} Z_{\omega_i}^{x_i} \right\}}_{=\delta_{x_i,0}} \\ &= \text{tr} \left\{ \frac{I + X_u}{2} Z_u P_u \right\} \delta_{x_0,1} \delta_{x_1,0} \dots \delta_{x_d,0} \\ &= -i[P = Y] \delta_{x_0,1} \delta_{x_1,0} \dots \delta_{x_d,0}. \end{aligned} \quad (\text{D45})$$

Hence, by substituting eq. (D45) into eq. (D44), we obtain

$$\xi(X, Z) = 0, \quad (\text{D46})$$

$$\xi(Y, Z) = -\sin(\gamma_{uv} w_{uv}) \prod_{\omega \in \mathcal{N}_u \setminus v} \cos(\gamma_{u\omega} w_{u\omega}). \quad (\text{D47})$$

- Case 3: $PQ = ZX, ZY$. This case is identical to Case 2, but with the vertices u and v swapped. Hence, from eq. (D46) and eq. (D47), we deduce that

$$\xi(Z, X) = 0, \quad (\text{D48})$$

$$\xi(Z, Y) = -\sin(\gamma_{uv} w_{uv}) \prod_{q \in \mathcal{N}_v \setminus u} \cos(\gamma_{vq} w_{vq}). \quad (\text{D49})$$

- Case 4: $PQ = ZZ$. This case is straightforward. One readily computes that $\xi(Z, Z)$ vanishes:

$$\begin{aligned} \xi(Z, Z) &= \text{tr} \left(\bigotimes_{j=1}^n \frac{1}{2}(I + X_j) Z_u Z_v \right) \\ &= \prod_{a \neq u,v} \text{tr} \left(\frac{I + X_a}{2} \right) \cdot \text{tr} \left(\frac{I + X_u}{2} Z_u \right) \cdot \underbrace{\text{tr} \left(\frac{I + X_v}{2} Z_v \right)}_{=0} \\ &= 0. \end{aligned} \quad (\text{D50})$$

From the above calculations, we see that for five of the nine choices of P and Q , $\xi(P, Q)$ vanishes: $\xi(Z, Z) = \xi(Z, X) = \xi(Y, X) = \xi(X, Z) = \xi(X, Y) = 0$. The remaining four non-vanishing ones are given by eq. (D42), eq. (D43), eq. (D47), and eq. (D49).

Step 3: Derivation of eq. (22)

We are now essentially done. By substituting the expressions for $\xi(P, Q)$ that we obtained in Step 2 into eq. (D11), and noting that $\mathcal{N}_{v \setminus u} = e$, $\mathcal{N}_{u \setminus v} = d$, $\mathcal{N}_{u \setminus \setminus v} = d \setminus F$, $\mathcal{N}_{v \setminus \setminus u} = e \setminus F$, and $N_{uv} = F$, we obtain eq. (22). \square

3. Proofs of Theorems 2 and 1

The analytical expressions for the expected cost function of both MA-QAOA and QAOA can be derived from XQAOA's analytical formula. Setting all α_i to 0 in eq. (22) gives eq. (18) in theorem 2. Moreover, setting all β_i to β and γ_i to γ in eq. (18) and simplifying gives eq. (13) in theorem 1.

4. Proof of corollary 4

Proof of corollary 4. By setting $\beta_k = 0$ for all k in eq. (22), we obtain the following expected cost function (corresponding to the edge $\{u, v\}$) for XQAOA₁^Y:

$$\langle C_{uv} \rangle_Y = \frac{w_{uv}}{2} - \frac{w_{uv}}{4} \sin 2\alpha_u \sin 2\alpha_v \prod_{\substack{w \in e \\ w \notin F}} \cos \gamma'_{wv} \prod_{\substack{w \in d \\ w \notin F}} \cos \gamma'_{uw} \left(\prod_{f \in F} \cos(\gamma'_{uf} + \gamma'_{vf}) + \prod_{f \in F} \cos(\gamma'_{uf} - \gamma'_{vf}) \right). \quad (\text{D51})$$

To prove corollary 4, we shall specialise eq. (D51) to unweighted graphs with odd edge degrees. First, we show that if every edge degree of a graph $G = (V, E)$ is odd, then the graph is necessarily two-colourable, i.e., there exists a map $\tau : V \rightarrow \{0, 1\}$ such that for all edges $\{u, v\} \in E$, $\tau(u) \neq \tau(v)$. Indeed, an instantiation of such a map τ is given by:

$$\tau(v) = \begin{cases} 0, & \deg(v) \text{ even,} \\ 1, & \deg(v) \text{ odd.} \end{cases} \quad (\text{D52})$$

It now remains for us to prove that τ is indeed a two-colouring: let $\{u, v\} \in E$. Note that the edge degree of an edge $\{i, j\} \in E$ is $\deg(\{i, j\}) = |\mathcal{N}(i) \cup \mathcal{N}(j)| - 2 = \deg(i) + \deg(j) - 2$. By our assumption, the edge degree $\deg(\{u, v\})$ is odd, and hence $\deg(u) + \deg(v)$ is also odd. This implies that exactly one of $\deg(u)$ and $\deg(v)$ is odd, from which it follows that exactly one of $\tau(u)$ and $\tau(v)$ is equal to 1. Hence, $\tau(u)$ and $\tau(v)$ cannot be equal to each other, i.e., $\tau(u) \neq \tau(v)$. This completes our proof that G is two-colourable.

Now, a graph is 2-colourable if and only if it does not contain an odd cycle (see [123, Theorem 5.21], for example). Hence, the graph G considered in corollary 4 with all edge degrees being odd must be triangle-free, i.e. G does not contain a 3-cycle. This implies that the set F in eq. (D51) must be empty.

Therefore, setting $F = \emptyset$, $w_{uv} = 1$, and $\gamma'_{ij} = \gamma_{ij}$ for all edges $\{i, j\} \in E$ gives the expected XQAOA₁^Y cost function (for the edge $\{u, v\}$) for unweighted graphs with all edge degrees being odd:

$$\langle C_{uv} \rangle_Y = \frac{1}{2} - \frac{1}{2} \sin 2\alpha_u \sin 2\alpha_v \prod_{w \in e} \cos \gamma_{wv} \prod_{w \in d} \cos \gamma_{uw}. \quad (\text{D53})$$

Note that if all the mixer unitary angles $\alpha_i = \alpha$ are equal and all the problem unitary angles $\gamma_{jk} = \gamma$ are equal, then eq. (D53) simplifies to

$$\langle C_{uv} \rangle_Y = \frac{1}{2} - \frac{1}{2} \sin^2 2\alpha \cos^{|e|+|d|} \gamma. \quad (\text{D54})$$

In eq. (D54), if one takes $\alpha = \frac{\pi}{4}$ and $\gamma = \pi$, one obtains

$$\langle C_{uv} \rangle_Y = \frac{1}{2} - \frac{1}{2} (-1)^{|e|+|d|}. \quad (\text{D55})$$

By assumption, G has only odd edge degrees. Therefore, $|e| + |d|$ is odd, which implies that

$$\langle C_{uv} \rangle_Y = \frac{1}{2} + \frac{1}{2} = 1. \quad (\text{D56})$$

So, the optimal expected cost function is given by

$$\sum_{\{u,v\} \in E} \langle C_{uv} \rangle_Y = |E|, \quad (\text{D57})$$

which coincides with the maximum cut size of 2-colourable graphs (the MaxCut of 2-colourable graphs is $|E|$ because one could just choose the maximum cut to be the 2-colouring).

Therefore, the approximation ratio achieved is 1, i.e., the XQAOA₁^Y state $|\gamma, \alpha\rangle$ provides the exact MaxCut solution for G . \square

5. Proof of corollary 5

In this appendix, we give a proof of corollary 5, which quantifies the advantage that XQAOA has over QAOA for an unweighted $(k+1)$ -vertex star graph $G = S_k$, illustrated in fig. 2. To keep our analysis general, we will take k to be an arbitrary positive integer for now and only later specialise to $k = 4$.

Note that when k is even, all the edge degrees in S_k are odd; hence, corollary 4 implies that XQAOA₁^Y with optimal angles computes the maximum cut of G with an approximation ratio of 1 whenever k is even. Hence, to complete the proof of corollary 5, it remains to show that QAOA₁ can do no better than achieve an approximation ratio of $3/4$.

To this end, consider the cost function for QAOA₁ given by eq. (14). For the star graph S_k , $|e| = |F| = 0$ and $|d| = k - 1$. Hence, eq. (14) reduces to $\langle C_{uv} \rangle = \frac{1}{2} + \frac{1}{4} \sin 4\beta \sin \gamma (1 + \cos^{k-1} \gamma)$, which is independent of the edge $\{u, v\}$. Therefore, the expected value of C can be written as

$$\langle C \rangle = \frac{k}{2} + \frac{k}{4} \sin 4\beta \sin \gamma (1 + \cos^{k-1} \gamma). \quad (\text{D58})$$

Maximising eq. (D58) over all β 's and γ 's gives

$$\begin{aligned} \langle C \rangle_{\max} &= \frac{k}{2} + \frac{k}{4} \max_{\gamma, \beta \in \mathbb{R}} [\sin 4\beta \sin \gamma (1 + \cos^{k-1} \gamma)] \\ &= \frac{k}{2} + \frac{k}{4} \max_{\beta \in \mathbb{R}} [\sin 4\beta] \max_{\gamma \in \mathbb{R}} [\sin \gamma (1 + \cos^{k-1} \gamma)] \\ &= \frac{k}{2} + \frac{k}{4} \max_{\gamma \in \mathbb{R}} g_k(\gamma), \end{aligned} \quad (\text{D59})$$

$$\text{where } g_k(\gamma) = \sin \gamma (1 + \cos^{k-1} \gamma). \quad (\text{D60})$$

To find the maximum point(s) of g_k , we start by taking its derivative. For $k \geq 2$, differentiating eq. (D60) and simplifying gives

$$g'_k(\gamma) = k \cos^k \gamma - (k-1) \cos^{k-2} \gamma + \cos \gamma, \quad (\text{D61})$$

which is a degree- k polynomial in $\cos \gamma$. Hence, finding the maximum point(s) of $g_k(\gamma)$ involves finding the roots of this polynomial. At this point, we specialise to $k = 4$. This allows to factorise the quartic polynomial eq. (D61) as

$$g'_4(\gamma) = 4 \cos^4 \gamma - 3 \cos^2 \gamma + \cos \gamma = \cos \gamma (\cos \gamma + 1) (2 \cos \gamma - 1)^2. \quad (\text{D62})$$

Hence, at a maximum point $\gamma^* \in \arg \max_{\gamma \in \mathbb{R}} g_k(\gamma)$, solving $g'_4(\gamma^*) = 0$ gives $\cos \gamma^* \in \{0, -1, \frac{1}{2}\}$. When $\cos \gamma^* = 0$, $g_4(\gamma^*) = \pm 1$; when $\cos \gamma^* = -1$, $g_4(\gamma^*) = 0$; and when $\cos \gamma^* = \frac{1}{2}$, $g_4(\gamma^*) = \pm \frac{9}{16} \sqrt{3} \approx \pm 0.974 < 1$. Taking the maximum of all these values gives $\max_{\gamma \in \mathbb{R}} g_k(\gamma) = 1$. Substituting this into eq. (D59) gives an approximation ratio of

$$\frac{1}{k} \langle C \rangle_{\max} = \frac{1}{2} + \frac{1}{4} \cdot 1 = \frac{3}{4}. \quad (\text{D63})$$

In conclusion, for the unweighted 5-vertex star graph S_4 , XQAOA₁^Y achieves an approximation ratio of 1, whereas QAOA₁ achieves an approximation ratio of at most $\frac{3}{4}$.